

Spin-orbit evolution of Mercury revisited

Benoît Noyelles

*Department of Mathematics and the Namur Centre for Complex Systems (NAXYS),
University of Namur, 8 Rempart de la Vierge, Namur B-5000 Belgium*
e-mail: benoit.noyelles@unamur.be ,

Julien Frouard

*Departamento de Estatística, Matemática Aplicada e Computação,
Instituto de Geociências e Ciências Exatas, Universidade Estadual Paulista (UNESP),
Avenida 24-A, Rio Claro, SP, CEP 13506-900 Brazil ,*
e-mail: frouard@rc.unesp.br ,

Valeri Makarov

US Naval Observatory, Washington DC 20392 USA
e-mail: vvm@usno.navy.mil

and

Michael Efroimsky

US Naval Observatory, Washington DC 20392 USA
e-mail: michael.efroimsky@usno.navy.mil

ABSTRACT

In the solar-system dynamics, Mercury presents a peculiar case, in that it is locked into the 3:2 spin-orbit resonance. Mercury's rotation period, 58 days, is exactly two thirds of its orbital period (88 days). No other example of a supersynchronous (higher than 1:1) spin-orbit resonance has been discovered in the Solar System so far.

It is widely accepted that the significant eccentricity of Mercury (0.206) favours the trapping into this resonance. More controversial is the question how

exactly the capture took place. In particular, a recent study by Makarov (2012) has demonstrated that entrapment into this resonance is certain if the eccentricity is larger than 0.2, provided that we use a realistic tidal model, the one which is based on the Darwin-Kaula expansion of the tidal torque, and which includes both the elastic rebound and anelastic creep of solids.

In our study, we revisit the scenario of Mercury’s capture into the supersynchronous spin-orbit resonances. The study is based on a realistic model of tidal friction in solids, a model that takes into account both the rheology of solids and the self-gravitation of the planet. Developed in Efroimsky (2012 a,b), the model was employed by Makarov et al. (2012), to determine the likely spin state of the planet GJ581 d, with its eccentricity evolution taken into account. The model was also used in the afore-cited work by Makarov (2012) to study the tidal spin-down and to find the likely end-state of a Mercury-like planet with its eccentricity fixed. We now continue this line of research, by taking into consideration the evolution of Mercury’s eccentricity. To that end, we consider realistic histories of the eccentricity, based on synthetic time evolution consistent with the expected statistics of the distribution of eccentricity.

We find that the realistic tidal model, as opposed to the commonly used constant time lag and constant phase lag models, changes dramatically the statistics of the probable final spin-orbit states. First, we have discovered that after only one crossing of the spin-orbit 3:2 resonance this resonance becomes the most probable end-state. Second, if a capture into this (or any other) resonance takes place, the capture is final, several crossings of the same state being forbidden by our model. Third, within our model the trapping of Mercury happens much faster than previously believed: for most histories, few tens of Myr are sufficient.

The swift capture justifies our treatment of Mercury as a homogeneous, unstratified body whose liquid core had not yet formed by the time of trapping.

Subject headings: Mercury — Resonances, spin-orbit — Rotational dynamics

1. Motivation

The rotation of Mercury is a special case in the Solar System dynamics. Half a century ago, radar observations determined the Mercurian spin period to be ≈ 58 days (Pettengill & Dyce 1965), which corresponds exactly to a 3:2 spin-orbit resonance. Later radar observations (Margot et al. 2007) demonstrated that the orientation of Mercury’s spin axis is consistent with the Cassini State 1 (Colombo 1965), the associated obliquity being

(2.04 ± 0.08) arcmin (Margot et al. 2012).

This dynamical configuration has long raised the question: how had Mercury been trapped into this resonance? There exists a consensus that the rather high eccentricity of Mercury (currently $e \approx 0.206$) favors the trapping by widening the resonance. At the same time, there exists a cleavage in opinion on whether the 3:2 resonance was the most likely end-state of Mercury’s spin-orbit evolution. Goldreich & Peale (1966) have estimated the capture probability as $\approx 7\%$, by using the so-called MacDonald’s torque (MacDonald 1964), a simplistic linear torque model later proven to be inherently inconsistent (Williams & Efroimsky 2012, Efroimsky & Makarov 2013) and also incompatible with the physically plausible rheology of terrestrial planets (Efroimsky 2012 a). In the same paper, Goldreich & Peale (1966) also obtained a probability bigger than 70%, for $e > 0.2$, by using the Darwin torque, a generic and perfectly legitimate model which, however, was combined in *Ibid.* with a frequency-independent k_2/Q assumption. The latter assumption later turned out to be in conflict with geodetic and seismic data (Efroimsky 2012 a), as well as with theoretical analysis of friction in solids (Karato & Spetzler 1990).

By taking into account the core-mantle friction, Peale & Boss (1977) explained that the 3:2 capture probability could be significantly enhanced, provided that Mercury has not been trapped into the 2:1 resonance prior to that. To prevent the 2:1 capture, the tidal quality factor Q should be smaller than 100, and the kinematic viscosity of the molten core of Mercury with a laminar boundary layer should be comparable to that of water, i.e., to be of the order of $0.01 \text{ cm}^2/\text{s}$. The role of the core-mantle friction was later revisited by Correia & Laskar (2009) who stated that, owing to the chaotic evolution of the eccentricity of Mercury, the planet might have been trapped into the 2:1 resonance before a decrease of the eccentricity disrupts this configuration. Later, these authors demonstrated in (Correia & Laskar 2010) that a past significant obliquity of Mercury should have lowered the probabilities of capture in all the higher spin-orbit resonances. An alternative scenario based on the observation of the impact craters suggests that Mercury may have had been in synchronous rotation, whereafter the rotation accelerated to meet the current 3:2 spin-orbit resonance (Wieczorek et al. 2012; Correia & Laskar 2012).

For a rigid Mercury, Correia & Laskar (2004) considered chaotic evolution of Mercury’s eccentricity, demonstrating that repetitive episodes of eccentricity increases could have boosted the probability of entrapment in the 3:2 resonance to 55%. A common problem in the aforementioned works is that they are based on a rheological model incompatible with the physical properties of actual terrestrial mantles (Efroimsky 2012a,b). A study based on a realistic tidal response was undertaken recently by Makarov (2012) who demonstrated that entrapment in 3:2 resonance is inevitable at eccentricities between 0.2 and 0.41, without

invoking a core-mantle friction or eccentricity variations.

These open issues motivated us to revisit the rotational history of Mercury, employing the same tidal model as Makarov (2012). Since the orbital eccentricity has a strong influence on rotation and tidal dissipation, we model its histories in a statistical way (Section 6). We incorporate these variations in our numerical simulations of the tidal and triaxiality-caused torques. Then we validate our methodology, by reproducing the results by Correia & Laskar (2004) (Section 7), before getting the updated statistics of capture into spin-orbit resonances up to 7:2 (Section 8).

The extremely swift capture obtained in our simulation serves as an *a posteriori* justification to our representation of the planet with a homogeneous sphere stratification whereof takes place well after the entrapment.

2. Proemial notes

Consider a planet spinning down due to the disturbance caused by its host star. The star exerts on the planet two torques. One, denoted with $\vec{\mathcal{T}}^{(\text{TRI})}$, is due to the planet's permanent triaxiality. Another torque, $\vec{\mathcal{T}}^{(\text{TIDE})}$, is caused by the tidal deformation of the planet. We shall assume that both torques are generated by the star only. The influence of other bodies in the Solar System is neglected.

Suppose that the planet is rotating about its major-inertia axis z ; and let θ be the sidereal angle of this rotation, reckoned from an arbitrary direction in inertial space. The evolution of the planetary spin will obey

$$\ddot{\theta} = \frac{\mathcal{T}_z^{(\text{TRI})} + \mathcal{T}_z^{(\text{TIDE})}}{C}, \quad (1)$$

C being the maximal moment of inertia, dot standing for time derivative, and the subscript z signifying the polar component of a torque.

As explained in the Appendix A, formula (A12), the tidal torque $\mathcal{T}_z^{(\text{TIDE})}$ can be expanded into a Fourier series, each term thereof being numbered with six integers $lmpqhj$. The torque consists of an oscillating and a secular part. The secular part is singled out by the condition $h = p$, $j = q$. So the secular part is represented with a much simpler series whose terms are numbered with four integers only: $lmpq$. An $lmpq$ term of the secular part of the torque turns out to be proportional to a product $k_l \sin \epsilon_l$, where k_l is the so-called dynamical Love number and ϵ_l is the phase lag. Both these quantities are functions of the Fourier mode ω_{lmpq} of the tides: $k_l \sin \epsilon_l = k_l(\omega_{lmpq}) \sin \epsilon_l(\omega_{lmpq})$. In neglect of the apsidal

and nodal motion, the Fourier tidal modes are approximated with

$$\omega_{lmpq} = (l - 2p + q) n - m \dot{\theta} \quad , \quad (2)$$

where n is the mean motion of the perturber, $\dot{\theta}$ is the spin rate of the perturbed body, $l \geq 1$ is an integer termed *the degree*, $m = 0, \dots, l$ is an integer known as *the order*; while p, q are two other integers (p varying from 0 through l , and q taking values from $-\infty$ to ∞).

It can also be demonstrated (Efroimsky 2012a,b) that, for realistic rheologies, the product $k_l(\omega_{lmpq}) \sin \epsilon_l(\omega_{lmpq})$ is an odd function of the mode. Among other things, this implies that the product (and, consequently, the $lmpq$ term of the secular part of the tidal torque) crosses a zero value and changes its sign when the Fourier tidal mode ω_{lmpq} goes through nil. From the expression (2), we see that these crossings (named *spin-orbit resonances*) take place when the dimensionless spin rate $\dot{\theta}/n$ transcends the rational values

$$\frac{\dot{\theta}}{n} = \frac{l - 2p + q}{m} \quad . \quad (3)$$

When the planet approaches such a resonance, it can either traverse it or be captured, depending on the specific trajectory in the phase space (i.e., depending on the initial conditions and on the presence or absence of chaos). Under these circumstances, capture becomes essentially probabilistic. The probability of entrapment (i.e., the share of the initial conditions resulting in capture) is defined by the dependence of $\mathcal{T}_z^{(\text{TRI})}$ and $\mathcal{T}_z^{(\text{TIDE})}$ on the orbital parameters and by the dependence of $\mathcal{T}_z^{(\text{TIDE})}$ on the tidal response of the despinning body. By the tidal response we imply the form of the functions $k_l(\omega_{lmpq}) \sin \epsilon_l(\omega_{lmpq})$, for all values of the degree l . In many practical situations, though, only the degree-2 inputs are relevant.

3. Overview of preceding studies

A method to estimate probabilities of capture was suggested by Goldreich & Peale (1966), for two extremely simplified models of the tidal torque. A clearer explanation of the method was presented in a later review by Goldreich & Peale (1968) to which we shall refer.

In one model considered in *Ibid.*, the torque was assumed to be linear in the tidal frequency. To be more precise, in the Fourier expansion of the torque over tidal modes, each torque component was set to be proportional to the appropriate tidal mode – see formula (19) in Goldreich & Peale (1968). The term *tidal mode* is more appropriate than *frequency*,

because a Fourier mode can assume either sign, while the physical frequencies are the modes’ absolute values and thus are positive definite.

Another model addressed in the said two works was the constant-torque one. Specifically, in the Fourier expansion of the torque over tidal modes, each torque component was set to be a constant multiplied by the sign of the corresponding mode – see Equation (29) in *Ibid.*

In their treatment of both models, Goldreich & Peale (1968) took into account only the secular, orbit-averaged, component of the tidal torque, and ignored the existence of an oscillating component. Below we shall test the validity of this approximation.

The surprisingly low probabilities of Mercury’s capture into the 3:2 resonance derived in these earlier studies were reassessed by Correia & Laskar (2004, 2009), still using the constant time-lag (linear in frequency) approximation. They noted that the orbit of Mercury underwent chaotic variations in the course of billions of years, likely resulting in significant changes of its eccentricity. The probability of capture into the 3:2 resonance is greatly enhanced for higher values of the eccentricity. Episodic increases in eccentricity up to 0.45 in their model helped to improve the chances of capturing Mercury into the state, in which it currently resides. Correia & Laskar (2004) performed 1,000 solutions for a representative sample of eccentricity curves, which resulted in 55.4% of the cases being eventually captured into the 3:2 resonance. The term “eventually” is important for the interpretation of these results. The constant time lag (CTL) model employed by Correia & Laskar allows the planet to leave a spin-orbit resonance higher than 1:1 by itself, if the eccentricity wanders out of a specific range where the resonance is stable. The departure from resonance can occur when the value of the tidal torque (which is pretty flat in the resonance’s vicinity in that model) becomes equal to the amplitude of the forced physical libration. Therefore, Correia & Laskar found numerous cases in their numerical simulations when Mercury was only temporarily locked into a supersynchronous resonance. Furthermore, a significant fraction of their trajectories (38.8%) ended up with a stable rotation rate of $\approx 1.2n$, where n is the mean orbital motion. One of the most dramatic predictions of the constant time lag model, which, to our knowledge, has never been confirmed by observation is the existence of stable pseudosynchronous states wherein the planet is locked into an average rotation at $(1 + 6e^2)n$. The constant time lag tidal torque vanishes at this rotation rate. Since Correia & Laskar’s eccentricity trajectories all converged to the current eccentricity value (0.20563) at the end of simulation, a pile-up of solutions close to the pseudosynchronous equilibrium should be expected.

In recent years, a more realistic model of tidal torques for terrestrial planets and moons emerged, which combines an anelastic Maxwell-type response of viscous medium with an

inelastic creep of solid materials (Efroimsky & Lainey 2007; Efroimsky & Williams 2009; Efroimsky 2012a). The approach is based on the well-known Fourier decomposition of the perturbing potential pioneered by Darwin (1879) and developed by Kaula (1964). The quality factor k_l/Q in each Fourier terms of this decomposition is replaced with a frequency-dependent rheological function, which will be further discussed in our paper. Numerical simulations with this more advanced tidal model become significantly more involved, and include a number of additional physical parameters. The pay-off is a much better and more accurate understanding of spin-orbit interactions and evolutions. Makarov (2012) employed this model to investigate a model exoplanet, which has the same parameters as the present-day Mercury. A series of limited-term numerical integrations of the planet spin rate with randomized initial conditions revealed that capture into the 3:2 resonance is by far the most likely outcome. In fact, the entrapment of the planet in this resonance is certain (100% probability) for eccentricities between 0.2 and 0.41, if the planet gets a chance of coming close to it. If Mercury decreased its spin rate from faster prograde rotations, it could have been captured at the 2:1 or even higher resonances. Makarov (2012) estimated the probability of capture into 2:1 at 23% for $e = 0.2056$. Generally, capture into supersynchronous resonances was found to be much more likely than with the tidal model used by Correia & Laskar (2004). It is important to note that all the analysis in (Makarov 2012) was done for a fixed, current value of eccentricity.

Furthermore, stable pseudosynchronous equilibria are ruled out with the realistic tidal model for planets like Mercury (Makarov & Efroimsky 2013). Therefore, the pile-up of end-states at $\dot{\theta}/n = 1 + 6e^2$ should never happen in reality. The tidal torque is much weaker at high tidal frequencies than in the CTL model, and it usually changes its sign in the close vicinity of resonances of interest. Therefore, being so much more efficient at capturing into a resonance, it is hardly capable of dragging a planet out of a resonance even if the eccentricity varies in a wide range. As was shown by Makarov (2012), a planet can cross a resonance only through a very small opening in the phase space, called “a needle’s eye” in that paper. In particular, the libration angle should be close to 90° at the periapse for that to happen. By the same argument, the libration angle should reach $\approx 90^\circ$ at the periapse for a captured planet to escape the resonance. Some force has to rock the planet very hard for that to happen, as the free libration is quite efficiently damped by the tidal torque.

4. Spin evolution of a planet subject to a tidal and triaxiality-caused torques

Consider a planet of a mean radius R , mass M_{planet} and the principal moments of inertia $A < B < C$. We shall effectively treat it as the primary body, while the star of mass

M_{star} will be playing the role of a secondary orbiting the primary and raising tides on it.

In many cases, including Mercury, one can assume that the spin of the planet is directed along its major-inertia axis z , the one related to the maximal moment of inertia C . The sidereal angle θ of the planet can be reckoned from the line of apsides to the largest-elongation axis x , the one related to the minimal moment of inertia A , as in Figure 1.

Expressing the maximal moment of inertia as $C = \xi M_{planet} R^2$, we shall rewrite the equation of motion (1) as

$$\ddot{\theta} = \frac{\mathcal{T}_z^{(\text{TRI})} + \mathcal{T}_z^{(\text{TIDE})}}{C} = \frac{\mathcal{T}_z^{(\text{TRI})} + \mathcal{T}_z^{(\text{TIDE})}}{\xi M_{planet} R^2} . \quad (4)$$

Here ξ is a dimensionless parameter whose value gives us an idea of the degree of inhomogeneity of the body. While for a homogeneous sphere the parameter assumes the value of 0.4, for the actual planet Mercury it is known to be $\xi = 0.346 \pm 0.014$, as obtained by Margot et al. (2012) and confirmed in Noyelles & Lhotka (2013). The fact that $\xi < 0.4$ indicates that the inner part of Mercury is denser than its outer part.

4.1. The triaxiality-caused torque

The polar component of the torque will be approximated with its quadrupole part (see, e.g., Danby 1962):

$$\mathcal{T}_z^{(\text{TRI})} = \frac{3}{2} (B - A) \frac{G M_{star}}{r^3} \sin 2\psi \quad (5a)$$

$$\approx -\frac{3}{2} (B - A) n^2 \frac{a^3}{r^3} \sin 2(\theta - f) . \quad (5b)$$

As usual, G denotes the Newton gravitational constant, r stands for the distance between the centres of mass of the two bodies, while M_{star} is the mass of the star (which, in our setting, is playing the role of a perturber effectively orbiting the tidally deformed primary, the planet). The mean motion is given by $n \equiv \sqrt{G(M_{planet} + M_{star})/a^3} \approx \sqrt{GM_{star}/a^3}$.

The notation ψ signifies the angle between the planetocentric direction towards the star and the minimal-inertia axis x , as in Figure 1. This angle ψ is equal to the difference between the planet’s true anomaly f , as seen from the star, and the planet’s sidereal angle θ , as measured from the line of apsides. These and other notations are listed in Table 1, the numerical values being presented in Table 2.

In practical computations, it is convenient to express the triaxiality-caused torque as a function of the mean anomaly \mathcal{M} . This will spare us of the necessity to compute of the

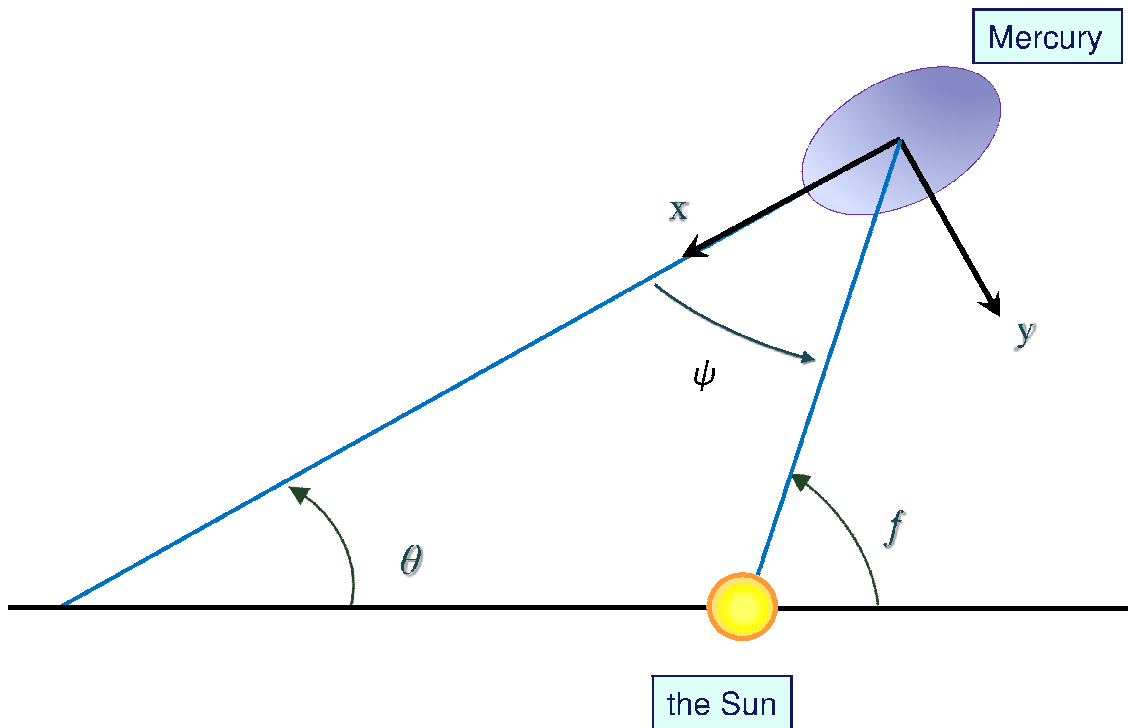


Fig. 1.— Horizontal line is that of apsides, so f is the true anomaly, θ is the sidereal angle of the planet, while $\psi = f - \theta$. The principal axes x and y of the planet correspond to the minimal and middle moments of inertia, respectively.

true anomaly f . To carry out this change of variables, we rewrite the expression (5b) as

$$\mathcal{T}_z^{(TRT)} = -\frac{3}{2} (B - A) n^2 \frac{a^3}{r^3} (\sin 2\theta \sin 2f - \cos 2\theta \cos 2f) \quad (6)$$

and insert therein the following formulae (see, e.g., Duriez 2002):

$$\left(\frac{a}{r}\right)^3 \cos(2f) = \sum_{k=-\infty}^{+\infty} X_k^{-3,2}(e) \cos(k\mathcal{M}) , \quad (7)$$

$$\left(\frac{a}{r}\right)^3 \sin(2f) = \sum_{k=-\infty}^{+\infty} X_k^{-3,2}(e) \sin(k\mathcal{M}) , \quad (8)$$

$X_k^{n,m}(e)$ being the classical Hansen coefficients. These are computed through the formula

$$X_k^{n,m}(e) = (1 + z^2)^{-n-1} \sum_{p=0}^{\infty} (-z)^p \sum_{h=0}^p C_{n+m+1}^{p-h} C_{n-m+1}^h J_{k-m+p-2h}(ke) , \quad (9)$$

where $z = (1 - \sqrt{1 - e^2})/e$, while C_b^a are the binomial coefficients, and $J_k(x)$ are the Bessel function of the first kind. The Hansen coefficients are related to the eccentricity polynomials via $G_{lpq} = X_{l-p+q}^{-(l+1), l-2p}$.

Altogether, formulae (6 - 8) entail:

$$\mathcal{T}_z^{(TRT)} = -\frac{3}{2} (B - A) n^2 \sum_{q=-\infty}^{+\infty} G_{20q}(e) \sin\left(2 \left[\theta - \left(1 + \frac{q}{2}\right) \mathcal{M}\right]\right). \quad (10)$$

In practice, the infinite series may be truncated to a sum over $q = -4, \dots, 4$. To our study, most relevant resonances are the 1:1, 3:2, 2:1, 5:2 and 3:1 ones, i.e., those corresponding to $q = 0, \dots, 4$. For $e > 0.3$, computation of the eccentricity function $G_{lpq}(e)$ requires a lot of computer time, as the convergence of the series (9) slows down. To bypass this problem, we computed these functions once for the whole range of eccentricities, and interpolated them during the computation, using cubic splines. To that end, the GNU Scientific Library (Galassi et al. 2009) was employed.

4.2. The tidal torque. General facts

Mathematical modeling of a tidal torque acting on a telluric body has long been subject to various misconceptions. One of them has it that certain rheologies should be regarded “unphysical”. The grounds for this belief were that $\mathcal{T}^{(\text{TIDE})} \propto k_2/Q$, wherefore a quality

Table 1. Symbol key

Notation	Description
ξ the moment of inertia coefficient of Mercury
R the radius of Mercury
$\mathcal{T}_z^{(\text{TRI})}$... the polar component of the triaxiality-caused torque acting on Mercury
$\mathcal{T}_z^{(\text{TIDE})}$ the polar component of the tidal torque acting on Mercury
M_{planet} the mass of Mercury
M_{star} the mass of the Sun
a the semimajor axis of Mercury
r the instantaneous distance between Mercury and the Sun
f the true anomaly of Mercury
e the orbital eccentricity
\mathcal{M} the mean anomaly of Mercury
C the maximal moment of inertia of Mercury
B the middle moment of inertia of Mercury
A the minimal moment of inertia of Mercury
n the mean motion
G Newton’s gravitational constant
τ_M the viscoelastic characteristic time (Maxwell time)
τ_A the inelastic characteristic time (Andrade time)
μ the unrelaxed rigidity modulus
J the unrelaxed compliance
α the Andrade parameter

Parameter	Notation	Numerical value
Semimajor axis	a	5.791×10^7 km
Mean motion	n	26.0879 rad/yr
Radius of Mercury	R	2440 km
Triaxiality of Mercury	$(B - A)/C$	1.2×10^{-4}
Dimensionless moment of inertia	$\xi \equiv C/(M_{planet} R^2)$	0.33333333
Ratio of masses of the Sun and Mercury	M_{star}/M_{planet}	6.0276×10^6
Maxwell time	τ_M	500 yr
Andrade time	τ_A	500 yr
Andrade parameter	α	0.2
Newton's gravitational constant	G	$66468 \text{ m}^3 \text{ kg}^{-1} \text{ yr}^{-2}$

Table 2: The numerical values of the parameters entering the model. The values of the triaxiality $(B - A)/C$ and dimensionless moment of inertia ξ were set the same as in Correia & Laskar (2004). The value of Mercury's radius R was borrowed from Archinal et al. (2011). The values of both the semimajor axis a and the mean motion n are secular, i.e., those obtained from the secular planetary theory of Bretagnon (1982). They are interrelated through $n = \sqrt{G(M_{star} + M_{planet})/a^3}$.

factor Q scaling as a positive power of the tidal frequency would render infinite values of the tidal torque in the zero-frequency limit. The misunderstanding stemmed from confusing the *seismic* quality factor Q with the *tidal* quality factors defined as $1/Q_l = \sin \epsilon_l$, where ϵ_l are phase lags. This misunderstanding is resolved by taking into account that the seismic quality factor reflects the rheology, while the tidal quality factors are defined by the interplay of rheology and self-gravitation, a circumstance that excludes unphysical divergencies in the quality functions $k_l/Q_l = k_l(\omega_{lmpq}) \sin \epsilon_l(\omega_{lmpq})$. As a result of another serious oversight, an expression for the torque, valid solely for the CTL model, was illegitimately employed by some authors in the constant angular lag context. Investigation of this wide-spread error can be found in Efroimsky & Makarov (2013).

One more, erstwhile common misconception which, too, made it to textbooks, was the belief in “pseudosynchronous” spin states of terrestrial planets and moons. While the possibility of such states for liquid bodies and bodies with oceans remains an open question, it has been explained in Makarov & Efroimsky (2013) that for solid objects such states are unavailable (or, to be exact, unstable and therefore always transient).

The consistent way of treating linear tides comprises two steps:

(1) Both the tide-raising potential of the secondary body (in our case, of the star) and the incremental tidal potential of the distorted primary (in our case, of the planet) must be expanded into Fourier series. The terms in both series are numbered with four integers $lmpq$.

(2) Each $lmpq$ term in the latter series should be related to its $lmpq$ counterpart in the former series. The interrelation implies introduction of the dynamical Love numbers k_l and phase lags ϵ_l as functions of a Fourier tidal mode ω_{lmpq} .

An $lmpq$ term of the induced tidal potential is proportional to the $lmpq$ term of the tide-raising potential, multiplied by some geometric factor and by the function $k_l \cos \epsilon_l = k_l(\omega_{lmpq}) \cos \epsilon_l(\omega_{lmpq})$. Similarly, an $lmpq$ term of the *secular part* of the tidal torque will be proportional to the $lmpq$ term of the tide-raising potential, multiplied by a geometric factor and by the so-called quality function $k_l \sin \epsilon_l = k_l(\omega_{lmpq}) \sin \epsilon_l(\omega_{lmpq})$. These results, now classical, were obtained by Kaula (1964). For a significant precursor, see Darwin (1879).

As was pointed out later in Efroimsky (2012a), the torque also contains an oscillating part, the expression for which is more complicated – see the explanation following the formula (A12) in the Appendix below.

The mode-dependencies of the Love numbers and tidal lags must be derived from the constitutive equation of the material of the perturbed body, with the effect of self-gravitation

taken into account. Instead, it has been common in the literature to use simplistic *ad hoc* models which render mathematically convenient mode-dependencies, however incompatible with physics. This often resulted not only in distortion of time scales, but also in serious qualitative misjudgments. In particular, Kaula (1964) and some other early authors believed in a frequency-independent $k_l \sin \epsilon_l$, an assumption incompatible with the Kramers-Kronig relations and certainly with the results of seismic and geodetic measurements. The erst-while popular CTL (constant time lag) model allows the emergence of the afore-mentioned “pseudosynchronous” spin states and also leads to considerable alteration of the probabilities of entrapment into spin-orbit resonances. Hence the necessity to reexamine the tidal entrapment process, employing a realistic rheology.

In this section, we shall lay the foundation for an accurate approach to the topic, by deriving a physics-based expression for the tidal torque acting on a terrestrial planet. Our treatment will be limited to the simpler case where the planet is not too close to the star ($R/a \ll 1$), the obliquity of the planet is small ($i \simeq 0$), and its eccentricity is not very large ($e < 0.4$). All three conditions are obeyed by Mercury now, and we have no reason to suspect that they were ever violated in the past.¹

As explained in detail in the Appendix A, under these assumptions the polar component of the tidal torque,

$$\begin{aligned} \mathcal{T}_z^{(TIDE)} = & \sum_{l=2}^{\infty} \left(\frac{R}{a} \right)^{2l+1} \frac{G M_{star}^2}{a} \sum_{m=1}^l \frac{(l-m)!}{(l+m)!} 2m \sum_{p=0}^l F_{lmp}(i) \sum_{q=-\infty}^{\infty} G_{lpq}(e) \\ & \sum_{h=0}^l F_{lmh}(i) \sum_{j=-\infty}^{\infty} G_{lhj}(e) k_l \sin \epsilon_l \cos [2(h-p)(\omega + \mathcal{M}) + (q-j)\mathcal{M}] \quad , \end{aligned} \quad (11)$$

can be approximated with

$$\begin{aligned} \mathcal{T}_z^{(TIDE)} = & \frac{3}{2} \frac{G M_{star}^2}{a} \left(\frac{R}{a} \right)^5 \sum_{q,j=-5}^5 G_{20q}(e) G_{20j}(e) k_2(\omega_{220q}) \sin \epsilon_2(\omega_{220q}) \cos [(q-j)\mathcal{M}] \\ & + O(e^6 \epsilon) + O(i^2 \epsilon) + O((R/a)^7 \epsilon) \quad , \end{aligned} \quad (12a)$$

where R and θ are the radius and sidereal angle of the planet, $\dot{\theta}$ is its spin rate, a and e are the semimajor axis and eccentricity of the star as seen from the planet. The notation

¹ In our modeling of Mercury’s orbital evolution, the eccentricity reached the values between $e = 0.4$ and $e = 0.45$ in only four histories out of a thousand, and over very limited time spans. This happened for three simulations covering 0.5 Gyr and for one simulation covering 0.1 Gyr.

$G_{lpq}(e)$ stands for the eccentricity polynomials. As ever, i denotes the inclination of the perturber on the equator of the perturbed body. Since in our case the role of the perturber is played by the star, i has the meaning of obliquity.

Be mindful that the moderate values of eccentricity allow us, in (11), to approximate an infinite series over q, j with a truncated, finite sum (12a). The details of the truncation can be found in the Appendix.

In the expressions (11) and (12a), the terms with $q = j$ constitute the secular part (given explicitly by the formula (A21) in the Appendix). The $q \neq j$ terms are oscillating. As explained in Section A.4 of the Appendix, while the oscillating part of the torque influences the fate of each particular trajectory, the overall statistics remains virtually insensitive to the oscillating part and is defined almost exclusively by the secular part (Makarov et al. 2012). Still, to be on the safe side, we employed in our computations the expression (12a) and not its secular version (A21b).

An $lmpqhj$ term of the torque contains a quality function $k_l(\omega_{lmpq}) \sin \epsilon_l(\omega_{lmpq})$. Here the dynamical Love numbers $k_l(\omega_{lmpq})$ are positive definite, and are even functions of the mode.² The phase lags $\epsilon_l(\omega_{lmpq})$ are odd functions, and their sign always coincides with that of the tidal mode ω_{lmpq} , as explained in Appendix A. Therefore, each factor $k_l(\omega_{lmpq}) \sin \epsilon_l(\omega_{lmpq})$ can be written as $k_l(\omega_{lmpq}) \sin |\epsilon_l(\omega_{lmpq})| \text{Sgn}(\omega_{lmpq})$. Hence the expression (12a) can be rewritten as

$$\begin{aligned} \mathcal{T}_z^{(TIDE)} = \frac{3}{2} \frac{GM_{star}^2}{a} \left(\frac{R}{a}\right)^5 \sum_{q, j=-5}^5 G_{20q}(e) G_{20j}(e) k_2(\omega_{220q}) \sin |\epsilon_2(\omega_{220q})| \text{Sgn}(\omega_{220q}) \\ \cos[(q-j)\mathcal{M}] + O(e^6\epsilon) + O(i^2\epsilon) + O((R/a)^7\epsilon) , \end{aligned} \quad (12b)$$

Through the medium of equation (2), each quality function $k_l(\omega_{lmpq}) \sin |\epsilon_l(\omega_{lmpq})| \text{Sgn}(\omega_{lmpq})$ becomes a function of the planetary spin rate $\dot{\theta}$:

$$\begin{aligned} k_l(\omega_{lmpq}) \sin |\epsilon_l(\omega_{lmpq})| \text{Sgn}(\omega_{lmpq}) \\ = k_l((l-2p+q)n - m\dot{\theta}) \sin |\epsilon_l((l-2p+q)n - m\dot{\theta})| \text{Sgn}((l-2p+q)n - m\dot{\theta}) , \end{aligned} \quad (13a)$$

where $((l-2p+q)n - m\dot{\theta})$ denotes a functional dependence on the argument $(l-2p+q)n - m\dot{\theta}$, not multiplication by a factor of $(l-2p+q)n - m\dot{\theta}$. In our simplified case,

² So it would be equally legitimate to write $k_l(\omega_{lmpq})$ as $k_l(\chi_{lmpq})$, where $\chi_{lmpq} \equiv |\omega_{lmpq}|$ are the positive definite physical forcing frequencies corresponding to the Fourier modes ω_{lmpq} .

(13a) becomes:

$$\begin{aligned}
 & k_2(\omega_{220q}) \sin |\epsilon_2(\omega_{220q})| \text{Sgn}(\omega_{220q}) \\
 &= k_2(2(n - \dot{\theta}) + qn) \sin |\epsilon_2(2(n - \dot{\theta}) + qn)| \text{Sgn}(2(n - \dot{\theta}) + qn) . \quad (13b)
 \end{aligned}$$

As a result, the entire sum (12a), or its equivalent (12b), can be interpreted as a function of $\dot{\theta}$. The mean motion and eccentricity will be treated as parameters whose evolution is much slower than that of $\dot{\theta}$.

In each term of the sums (12a) and (12b), the factor $k_2 \sin \epsilon_2 = k_2 \sin |\epsilon_2| \text{Sgn}(\omega_{220q})$, expressed as a function of $\dot{\theta}$, has the shape of a kink, as shown on Figure 2. The shape ensues from interplay of rheology (which dominates at higher frequencies) and self-gravitation (which takes over in the zero-frequency limit), see the Appendix B and references therein. The emergence of this shape is natural, for each term should transcend zero and change its sign *continuously* when the rotation rate goes through the appropriate spin-orbit resonance.

In the sums (12a) and (12b), the kink-shaped factors $k_2 \sin \epsilon_2$ have different multipliers $G_{20q}^2(e)$. Therefore, the expression (12b), treated as a function of $\dot{\theta}$, will be a superposition of many kinks of different magnitudes. In our case, summing over $-5 \leq q \leq 5$, we included ten terms, since $G_{20,-2}(e)$ vanishes identically. The kinks will be centered at different resonant values of $\dot{\theta}$. The resulting curve depicting the overall sum (12) will cross zero in points *very close* to the commensurabilities $\dot{\theta} = n(1 + q/2)$, but not exactly in these commensurabilities — like the little kink near $\dot{\theta}/n = 3/2$ in Figure 3.³

Sitting on the right slope of a more powerful kink (the one with $q = 0$), the little kink (corresponding to $q = 1$) experiences a vertical displacement called *bias*. Although the bias of the little kink is caused by all the other kinks, the influence of its left neighbour is evidently dominant. The vertical bias of the little kink in Figure 3 is a feature immanent to any spin-orbit resonance, if the eccentricity is non-zero. The zero-eccentricity case is exceptional because, in the quadrupole approximation,⁴ it comprises only one component of the tidal torque, the semidiurnal one (corresponding to the principal tidal frequency ω_{2200}).

³ As ensues from (11) and (13a), the $lmpq$ term of the secular part of the torque is decelerating for $\omega_{lmpq} < 0$ and is accelerating for $\omega_{lmpq} > 0$. This observation, combined with the expression (2), explains why the $lmpq$ term of the secular torque is negative on the right of the $lmpq$ resonance and positive on its left — see the two kinks depicted in Figure 3.

⁴ In higher-degree approximations, we would be taking into account the $lmpq$ terms with $l > 2$. However, from the tables of the $F(i)$ and $G(e)$ functions, it can be observed that only the terms with $q = p = l - m = 0$

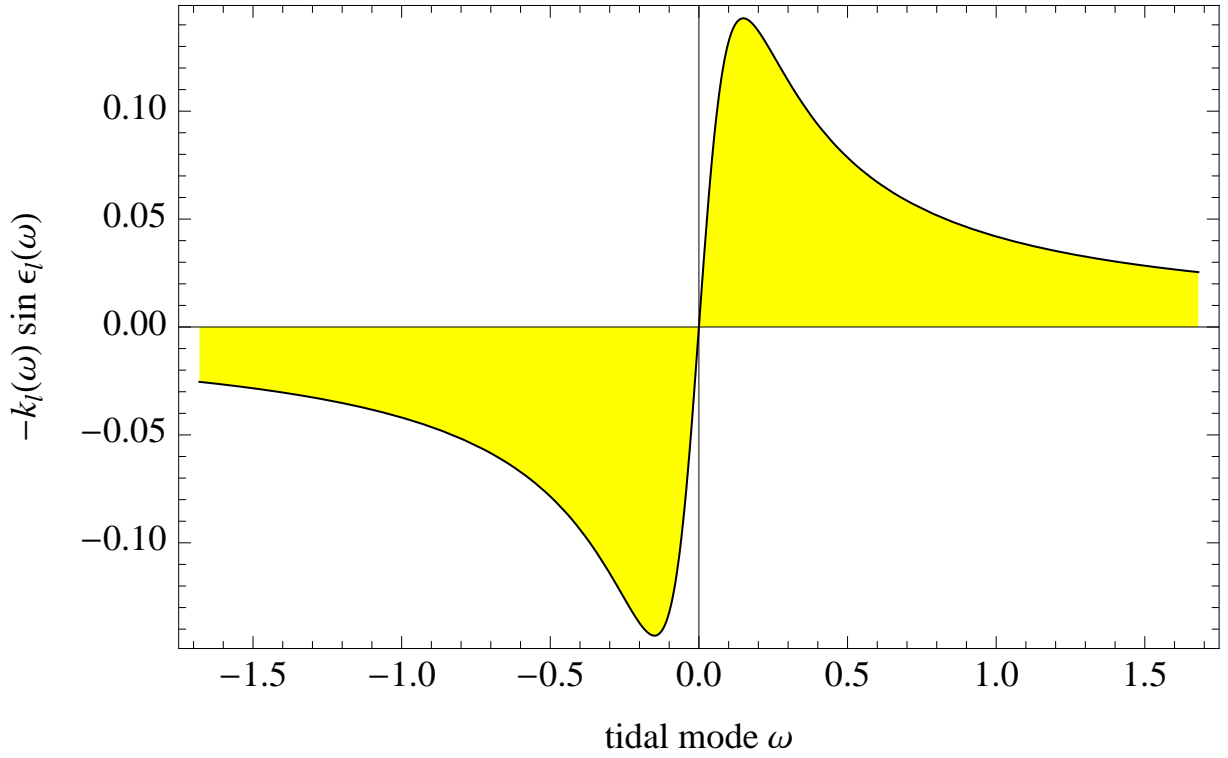


Fig. 2.— A typical shape of the quality function $k_l(\omega) \sin \epsilon_l(\omega)$, where ω is a shortened notation for the tidal Fourier mode ω_{lmpq} .

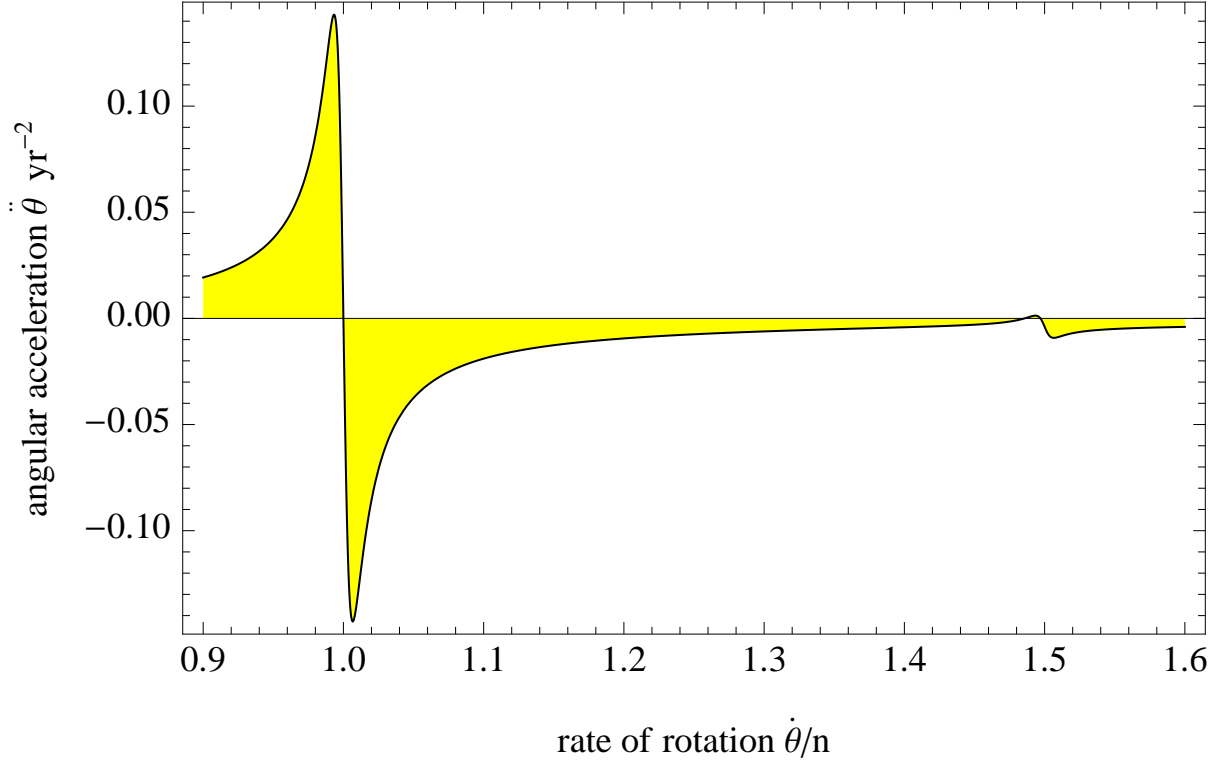


Fig. 3.— The angular acceleration provided by the secular part of the tidal torque. The torque is expanded into the Darwin-Kaula series and expressed as a function of the dimensionless spin rate, $\dot{\theta}/n$. The left kink comes from the leading, semidiurnal term $\{lmpq\} = \{2200\}$. It is centered in the point $\dot{\theta}/n = 1$ corresponding to the 1:1 spin-orbit resonance. The right kink comes from the term with $\{lmpq\} = \{2201\}$, which is vanishing in the 3 : 2 resonance. The right kink is considerably displaced vertically, owing to the bias provided by the slopes of the other kinks, mainly by the leading, semidiurnal kink.

A constant bias of the secular torque was also considered by Goldreich & Peale (1968), who pointed out its crucial role in the capture probability calculation. However, in our model the bias has a physical meaning very different from that in the CTL model. In our case, the bias is generated by the non-vanishing inputs from the non-resonant modes called into being by the non-uniform orbital motion. Without these non-vanishing bias terms, capture into a spin-orbit resonance would be inevitable, and the tidal dissipation would completely cease once the rotator is locked in the resonance. Near a resonance q' , the spin rate $\dot{\theta}$ is close to $n(1 + q'/2)$, and the right-hand side of the sum (12b) can be conveniently decomposed into two parts. The first one is the $q = q'$ term, a kink-shaped function transcending zero at $\dot{\theta} = n(1 + q'/2)$. The second part, *bias*, is constituted by all the $q \neq q'$ terms of the sum. This way, the bias is the input of all the $q \neq q'$ terms into the values assumed by the overall torque in the vicinity of the $q = q'$ resonance. In the said vicinity, the bias is a slowly changing function, which can, to a good approximation, be treated as constant. For not too large eccentricities, the bias is usually negative – this is why the little kink in Figure 3 is shifted downwards.

As mentioned above, the $q = q'$ term assumes a zero value at $\dot{\theta}/n = (1 + q'/2)$. However, the bias displaces the location of the zero. For example, the 3:2 kink in Figure 3 goes through nil in a point located a bit to the left of $\dot{\theta}/n = 3/2$. Being extremely small, the shift of the equilibrium away from the exact resonance frequency has no practical consequences, since the net nonzero tidal torque is compensated by an opposing secular triaxiality-caused torque, as explained in Makarov & Efroimsky (2013).

4.3. The tidal torque and the role of rheology

In the preceding section we determined that the overall tidal torque (12), taken as a function of the spin rate $\dot{\theta}$, will be a superposition of kinks. Figures 2 and 3 depicted a typical kink and the way kinks superimpose in the sum. Serving purely illustrative purposes, those two figures were not generated for any realistic set of parameters relevant to the actual planet Mercury. Each kink was intentionally stretched horizontally, its extrema being conveniently spread apart, to emphasise that the transition through nil is continuous.

Analogous figures for realistic parameters of Mercury would have sharper features, like in Figure 4. Despite the sharp-looking peaks, the dependency is continuous, and the middle

come out non-vanishing for $e = i = 0$. In the quadrupole approximation, the sole surviving term will be $\{lmpq\} = \{2200\}$, while in a higher-degree approximation we would get the extra modes with $\{lmpq\} = \{ll00\}$, for each l included.

part has a finite slope, even though on the picture it looks almost vertical. The form of the

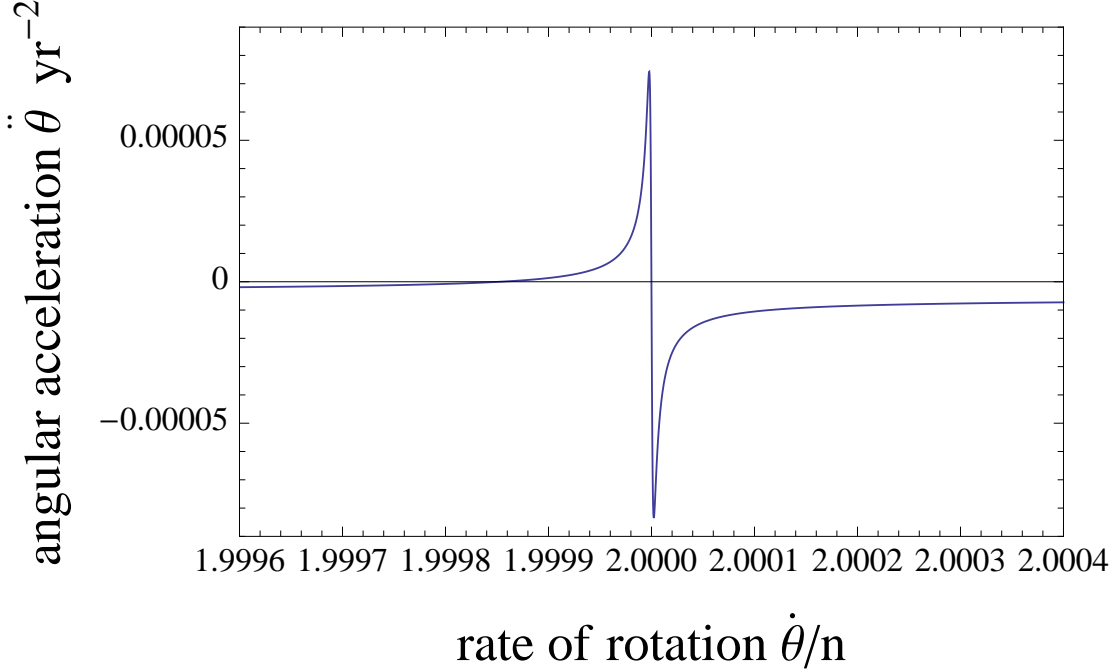


Fig. 4.— Angular acceleration of Mercury caused by the secular tidal torque (12), in the vicinity of the 2:1 spin-orbit resonance.

plot is dictated by the shape and magnitudes of the quality functions $k_l(\omega_{lmpq}) \sin \epsilon_l(\omega_{lmpq})$ expressed as functions of the spin rate via formulae (13). The quality functions show up in each term of the tidal torque, and the shapes of these functions are crucial for determining the probabilities of entrapment. The shapes are defined by the size and mass of the body and by its rheological properties. The rheological properties are accounted for by a constitutive equation, i.e., a by law interconnecting the strain and stress. Within linear rheologies, a constitutive equation can be rewritten in the frequency domain where each Fourier harmonic $\bar{u}_{\gamma\nu}(\chi)$ of the strain gets expressed, algebraically, as the appropriate harmonic of the stress $\bar{\sigma}_{\gamma\nu}(\chi)$ multiplied by the complex compliance $\bar{J}(\chi)$ appropriate to this harmonic:

$$2 \bar{u}_{\gamma\nu}(\chi) = \bar{J}(\chi) \bar{\sigma}_{\gamma\nu}(\chi) , \quad (14)$$

$\chi = \chi_{lmpq}$ being the physical forcing frequency, and $\gamma\nu$ being the tensorial indices. The relation (14) is an exact analogue to a complex harmonic of current written as the appropriate harmonic of voltage, multiplied by the inverse complex impedance. The roles of the current, voltage and inverse impedance are played by $2 \bar{u}_{\gamma\nu}(\chi)$, $\bar{\sigma}_{\gamma\nu}(\chi)$ and $\bar{J}(\chi)$, correspondingly.

The complex compliance $\bar{J}(\chi)$ contains in itself all information about the response of the material, under the assumption that the material is isotropic. Modeling the mantle

rheology, i.e., deriving $\bar{J}(\chi)$, we rely on a combined model which is Andrade at higher frequencies and Maxwell in the low-frequency limit. As was demonstrated in Efroimsky (2012a,b), the mathematical formalism of the Andrade model can be modified in a manner permitting a switch to the Maxwell model at low frequencies. The necessity for this switch originates from the fact that at different frequencies different physical mechanisms dominate the internal friction.

After the compliance $\bar{J}(\chi)$ is found, it may be employed to determine the tidal response of the planet, i.e., the quality functions $k_l(\omega_{lmpq}) \sin \epsilon_l(\omega_{lmpq})$. Carrying out this part of the problem, we assumed that the larger part of tidal dissipation of energy is taking place in the mantle, and we approximated the planet with a homogeneous ball endowed with the rheological properties representative of the mantle. Despite the evident simplification, the model is likely to reflect the qualitative features of the spin-orbit interactions, and to entail a reasonable comparison of the entrapment probabilities for different resonances. The main qualitative feature faithfully represented by the model is the kink shape of the terms in the expansion of torque.

Further improvement of the model and its enrichment with details (friction between layers, etc) will certainly alter the magnitude and detailed shapes of the kinks. It is however highly improbable that the basic kink shape varies considerably (though it may, in principle, acquire secondary ripples due to interaction between the layers of the planet).

With all these assumptions taken into account, the complex compliance can be used to write down the functions $k_l(\omega_{lmpq}) \sin \epsilon_l(\omega_{lmpq})$, as shown in Efroimsky (2012a,b). An extremely squeezed account of the method can be found below in Appendix B.

5. Characteristic time of despinning

Before we start integrating the ordinary differential equation (4), it is of both theoretical and practical interest to estimate the characteristic time scale of the secular deceleration. This time scale is greatly influenced by the tidal dissipation rate which, in its turn, is dependent on the instantaneous rate of rotation, on the ratio of planet's radius R to the orbital separation a , on the eccentricity e , and on other physical parameters. Theoretical studies tell us that some of the Solar System bodies spin down relatively quickly, on the time scale of 10^5 - 10^6 yr (e.g., the Moon), while others seem to need time intervals comparable to their lifetime, to slow down appreciably (Castillo-Rogez et al. 2011). The practical side of the issue is the required computing time, which may be prohibitively long for a definite result to be obtained. (Naturally, the longer it takes to despin, the more computing time is

needed.)

Following the established tradition, (e.g., Rasio et al. 1996), we define a characteristic time of despinning as

$$\tau_{\text{despin}} = \frac{|\dot{\theta}|}{|\ddot{\theta}|} . \quad (15)$$

Representing a time span over which the spin rate decreases considerably, this quantity should not be taken for the actual time it takes the planet to spin down from a given $\dot{\theta}$ to, say, the synchronous rotation state. The actual time of despinning can be obtained only by numerical integration of the differential equation (4).

The decimal logarithms of characteristic spin-down times are shown in Figure 5 for three values of eccentricity, $e = 0.1$ (upper curve), $e = 0.2056$ (middle curve), and $e = 0.3$ (lower curve). Generally, the characteristic times are of the order of 10^7 yr or longer, while the integration step size has limitations imposed by the kink shape of the tidal torque components.⁵ Integrating the dynamical equation for 10^7 yr with a small step is computationally very expensive. For this reason, we present in Section 8.1 the results of 1,000 simulations, in which the tides have been artificially accelerated by a factor of 16. Other computations support the validity of these results.

6. Numerical modeling of the history of Mercury’s eccentricity

6.1. Background

Classical methods to investigate the past orbital history of Mercury⁶ rely either on numerical integrations of the planetary complete equations of motion (Quinn et al. 1991; Batygin & Laughlin 2008; Laskar & Gastineau 2009) or on numerical integration of their averaged counterparts (Laskar 1988), or on fully analytical approximations (Bretagnon 1974). In this section, we present a method employed by us to obtain the eccentricity history of

⁵ When the planet traverses a low-order resonance, a considerable slow-down occurs due to the left shoulder of the appropriate tidal kink. In Figures 3 and 4, the right shoulder of each kink is, typically, negative (decelerating), while the left shoulder of each kink is, typically, positive (accelerating). We prefer to say ‘*typically*’, because there may exist situations where a kink corresponding to a higher resonance is located, fully or partially, below the horizontal axis – see the small kink in Figure 3. Even though, despinning leftwards through this kink will result in a decrease of the overall despinning action of the tidal torque.

⁶ We also note an effective secular method which was developed by Boué et al. (2012) and was published posteriorly to our numerical integrations.

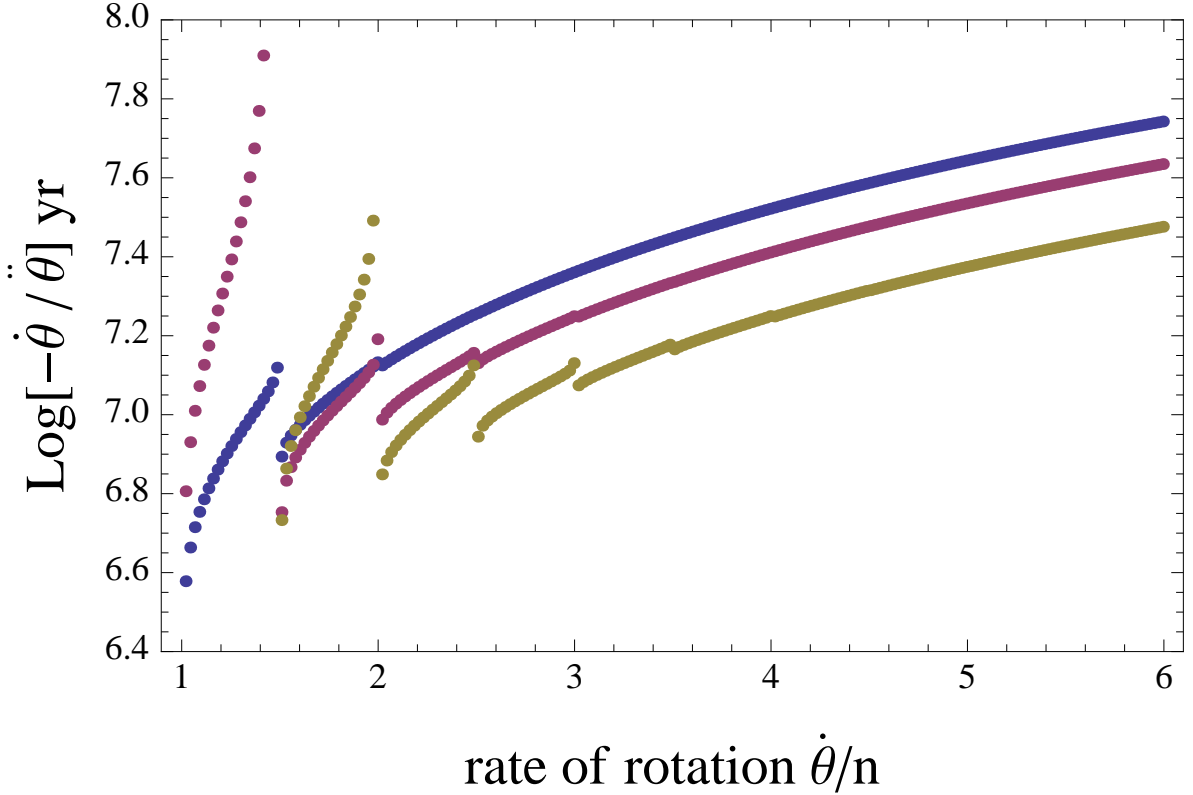


Fig. 5.— Decimal logarithm of the characteristic spin-down time of Mercury as a function of the rotation rate, for three values of eccentricity, $e = 0.1$ (upper curve), $e = 0.2056$ (middle curve) and $e = 0.3$ (lower curve). The curves are computed for discrete sets of points, to avoid the resonances. For all values of the eccentricity, Mercury’s spin is accelerating when $\dot{\theta}/n < 1$ (not shown in this figure). For sufficiently large eccentricities, the spin may be accelerating also over some spans of values of $\dot{\theta}/n$ larger than unity. For example, for the value $e = 0.3$, the spin is accelerating when $\dot{\theta}/n \in [1, 1.5)$. It is for this reason that the segment of $\text{Log}[-\dot{\theta}/\ddot{\theta}]$ between $\dot{\theta}/n = 1$ and $\dot{\theta}/n = 1.5$ is not plotted here. At this eccentricity, the secular acceleration, $\ddot{\theta}$ is positive for $\dot{\theta}/n < 1.5$.

Mercury over Gyr timescales. The method is based on the statistical formulae developed in Laskar (2008).

The Solar System has been shown to be chaotic (Nobili et al. 1989; Laskar 1989; Sussman & Wisdom 1992), and numerical simulations show that no precise solution can be obtained by integration back in time over ~ 50 Myr or longer (Laskar et al. 2011). Statistical considerations over a large number of possible orbits are thus needed.

Within the statistical approach, Laskar (2008) studied the possible orbital history of Mercury, using the averaged planetary equations. His dynamical model contains the eight planets, with their mutual secular gravitational perturbations obtained through a second-order perturbation method, along with perturbations from the General Relativity and the Moon (Laskar 1986). Note that the averaged equations imply constant secular semi-major axes of the planets. After numerical integration of a large number of histories of the Solar System over 5 Gyr, starting with very close initial conditions, some statistics can be obtained about the values of the eccentricity and inclination of each planet over this timespan. In particular, the eccentricity of Mercury e statistically follows a Rice density function (see Laskar 2008):

$$f_{T,m}(e) = \frac{e}{\sigma^2} \exp\left(-\frac{e^2 + m^2}{2\sigma^2}\right) I_0\left(\frac{em}{\sigma^2}\right), \quad (16)$$

where the parameter σ obeys the approximation

$$\sigma^2(T) = b_0 + b_1 T \quad (17)$$

corresponding to a diffusion process, with $b_0 = 2.07 \times 10^{-3}$, $b_1 = 1.043 \times 10^{-3}$, $m = 0.1875$, and with T being the time in Gyr. The notation I_0 stands for the modified Bessel function of the first kind. This function is often approximated by a series expansion, but in the case of large values of ν it is adequately approximated with an exponential function (Press et al. 1992). It is important to note that m and σ are not the mean and standard deviation of the Rice distribution.

6.2. Method

Our goal here is to produce a synthetic time series of Mercury’s eccentricity, based on the density function (16). To this end, we use a simple Wiener process (or a Brownian motion) of the type

$$e(T + \delta_t) = e(T) + \sigma(\delta_t) \delta_e, \quad (18)$$

where $e(0)$ corresponds to the initial eccentricity and σ is the standard deviation. Each of the eccentricity values are separated in time by a constant time step δ_t , and the process has

independent and stationary increments δ_e . For a Wiener process, the increments δ_e obey a Gaussian distribution $\mathcal{N}(0, 1)$.

To obtain the standard deviation needed in (18), we fit a Gaussian distribution

$$f(e; \mu, \sigma^2) = \frac{1}{\sqrt{2\pi\sigma^2}} \exp\left[-\frac{(e - \mu)^2}{2\sigma^2}\right] \quad (19)$$

to the Rice density function (16). The standard deviation of the Gaussian distribution corresponds to $\sigma^2(t) = 0.0009t$. We then applied a few corrections to the time series.

First, the Rice density has a characteristic drift of its mean value and most probable value over time. In order for the Gaussian distribution to still maintain a good fit in the complete time interval, this can be compensated by adding a small drift $D = 0.0023T$ to the value of the eccentricity at a time T . By fitting the drift, we obtain an initial mean $\mu = 0.1876$, which will be used also for the initial value $e(0)$.

Secondly, we make a change of the timescale: $T^* = T + 2.33$ Gyr. This step is necessitated by the fact that the first 250 Myr of integration computed by Laskar (2008) have a very different slope of $\sigma^2(t)$, and have not been taken into account in his fit of (16) – see Laskar (2008, Figure 15b). To be able to fit the Rice distribution with its current parameters for all values of T , a Gaussian distribution with a standard deviation linear in time has to start at an initial time of -2.33 Gyr. Also, due to the lack of information about the first 0.5 Gyr of evolution, we keep only the part corresponding to the interval $T^* \in [0.5, 4]$ Gyr.

One of the discrepancies between the Rice distribution and the Gaussian distribution lies in the distribution of very low eccentricity values. The Rice density is defined in the range $[0, +\infty]$ and its distribution for low e tends to be more linear with increasing T . On the other hand, the Gaussian distribution is defined on $[-\infty, +\infty]$, allowing the possibility of negative eccentricities, and is completely symmetric with respect to its mean value. Although, we can see from Laskar (2008) that the eccentricity distribution of Mercury does not show a strong linear behaviour for low e (which is not the case for the other planets of the Solar System). The orbits which have $e < 0$ at any time during the 3.5 Gyr time span have been discarded from the final results, with the side effect of slightly depleting the distribution of low e , compared to a non-modified Gaussian distribution.⁷ We have checked that it does not introduce any bias, since this reduced distribution matches the Rice distribution for low

⁷ Synthetic orbits obtained via the Brownian-motion method can have negative eccentricities. While the Rice distribution prohibits this, the Gaussian distribution does not.

e even more closely. Figure 6 shows the Rice distribution function for $T = 1$ Gyr computed with the equation (16), compared with the distribution of 500,000 synthetic orbits obtained through the process (18).

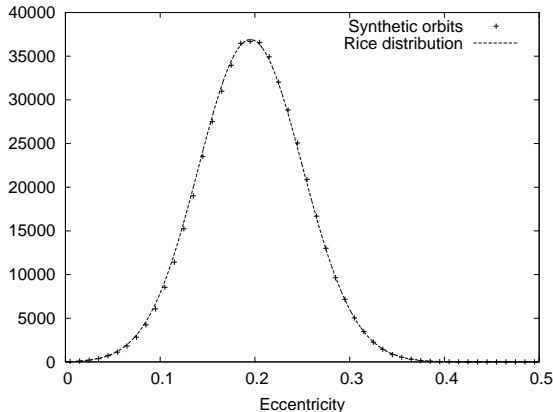


Fig. 6.— The Rice distribution function for $T = 1$ Gyr from Eq.16 (line) and its approximation obtained from the distribution of 500,000 synthetic orbits evolved for 1 Gyr with the process of Eq.18 (points).

Our third correction concerns the time direction. The secular planetary equations used by Laskar (2008) are perfectly time-reversible and have been used to explore the past orbital history of Mercury by Correia & Laskar (2004) over 4 Gyr. The process described above can then be applied by only reversing its time evolution (see some examples in Figure 7).

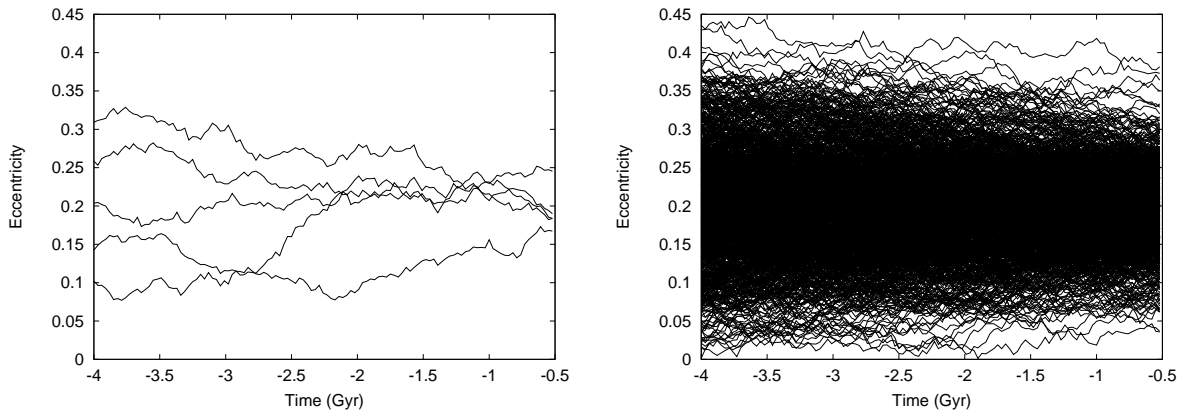


Fig. 7.— Evolution over time of five and one thousand synthetic orbits obtained with the Wiener process (Eq.18).

We have to keep in mind that these statistics are an approximation to the evolution trajectories given by the secular planetary equations of motion, and that low eccentricities

are considered as rare events. For example, employing the tidal model from Correia & Laskar (2004) and setting $T = -4$ Gyr, we obtained the following probabilities of e attaining the critical values needed to destabilise some spin-orbit resonances: $P(e < e_{5/2} = 0.024877) = 0.925\%$, $P(e < e_{2/1} = 0.004602) = 0.43\%$ and $P(e < e_{3/2} = 0.000026) = 0.365\%$. These are estimates obtained from the Gaussian distribution; the Rice distribution gives slightly smaller values.

7. Numerical simulation of Mercury’s spin rate

7.1. Methodology

Our next goal is to explore the influence of the tidal model on the probability of capture into spin-orbit resonances, in the specific context of Mercury. Makarov (2012) has recently accomplished this work for a constant eccentricity. Here we use our synthetic trajectories to include the statistical variations of Mercury’s eccentricity in the study. We will build statistically relevant samples of simulations of the despinning of Mercury, with two kinds of tidal model: the one from Correia & Laskar (2004) and our model (12b).

Our numerical simulations are based on integration of the differential equation (4) for the spin rate of Mercury. The torques entering this equation depend on the eccentricity which is calculated, at each step, from the synthetic distribution. The value of the eccentricity at a given time is estimated, through cubic spline interpolation, from the synthetic evolution trajectory sampled at a regular grid of time points. More detail on this method can be found in (Dahlquist & Björck 2008). The error associated with this interpolation is of the 4th order (Sonneveld 1969), i.e., a decrease of the sampling step of the trajectory by a factor of α will reduce the interpolation error by a factor of $\approx \alpha^4$. For generating eccentricities, we used the interpolation routines from the GNU Scientific Library (Galassi et al. 2009). The numerical integrator was the Adams-Bashforth-Moulton 10th-order predictor-corrector scheme (Hairer et al. 1987). Through the simulations, the value of the mean motion was kept constant: $n = 26.0878$ rad/yr.

7.2. Reproducing the results from Correia & Laskar (2004)

This part aims at checking the reliability of our method in trying to reproduce the results of Correia & Laskar (2004). These authors ran 1,000 numerical simulations of the spin-rate history of Mercury, starting with a spin period of 20 days and finishing with the current period of 87.9 days. Those authors integrated equation (4) with the following expression

for the tidal torque (sometimes referred to as the ‘*viscous model*’):

$$\mathcal{T}_z^{(TIDE)} = -\mathcal{Z} \left[\dot{\theta} \mathcal{A}(e) - n \mathcal{N}(e) \right] , \quad (20)$$

$$\mathcal{A}(e) = \left(1 + 3e^2 + \frac{3}{8}e^4 \right) (1 - e^2)^{-9/2} , \quad (21)$$

$$\mathcal{N}(e) = \left(1 + \frac{15}{2}e^2 + \frac{45}{8}e^4 + \frac{5}{16}e^6 \right) (1 - e^2)^{-6} , \quad (22)$$

$$\mathcal{Z} = \frac{3n M_{star} k_2}{\text{“}Q\text{”}(n)} \frac{R^5}{a^3} . \quad (23)$$

Accordingly, the tidally produced contribution into the angular acceleration reads as:

$$\ddot{\theta}^{(TIDE)} = \frac{\mathcal{T}_z^{(TIDE)}}{C} = \frac{\mathcal{T}_z^{(TIDE)}}{\xi M_{planet} R^2} = -\mathcal{K} \left[\dot{\theta} \mathcal{A}(e) - n \mathcal{N}(e) \right] , \quad (24)$$

$$\mathcal{K} = \frac{3n}{\xi} \frac{k_2}{\text{“}Q\text{”}(n)} \left(\frac{R}{a} \right)^3 \frac{M_{star}}{M_{planet}} , \quad (25)$$

with $\mathcal{K} = 8.45324 \times 10^{-7} \text{ yr}^{-1}$, $\xi = 0.3333$, $k_2 = 0.4$, $\text{“}Q\text{”}(n) = 50$. They modeled the evolution of Mercury’s eccentricity by integration, back in time, of 1,000 orbits over 4 Gyr.

The formulae (20 - 25) are based on the assumption that the time lag bears no dependence upon frequency. Hence the name: the constant time lag (CTL) model. Detailed derivation of these formulae can be found in the Appendix to Williams & Efroimsky (2012). In various forms, this result appeared much earlier in Hut (1981) and Eggleton et al. (1998). In an implicit form, it was pioneered by Goldreich & Peale (1966, Equation 24).

Although the quantity Q is used in Correia & Laskar (2004) without quotation marks, we find these marks necessary and introduce them in (23) and (25), in order to emphasise that this quantity is *not* a tidal quality factor. We also endow it with an argument (n), to remind that, within the CTL model, $\text{“}Q\text{”}(n)$ is a function of the mean motion. For details and references, see Appendix C below.

Numerical simulations based on the formulae (20 - 25) rendered three types of capture:

- Type I: Mercury is trapped into the 3:2 spin-orbit resonance as soon as the spin rate reaches $1.5n$ (31 occurrences out of 1,000 orbits).

- Type II: Mercury crosses once the spin-orbit resonance without being trapped, but the value of the eccentricity e prevents the planet from further despinning, with $\dot{\theta}$ remaining greater than $1.4n$. As a consequence, the spin crosses the resonance several times, until it becomes trapped (168 occurrences).
- Type III: Late capture. The spin crosses the resonance and keeps going down, reaching a frequency close to n . Then, as a consequence of the chaotic orbital dynamics of Mercury, the eccentricity becomes greater and increases the spin rate, inducing crossings of the 3:2 spin-orbit resonance, until the planet is finally trapped (355 occurrences).

The linear tidal model (20) implies that the spin rate cannot be smaller than an equilibrium value $\dot{\theta}_{eq} > n$, which is called pseudosynchronous rotation. As a consequence, the synchronous rotation can not be reached, unless the eccentricity drops to very small values, and the difference between the pseudosynchronous spin rate $\dot{\theta} = (1 + 6e^2)n$ and the synchronous one $\dot{\theta} = 1n$, becomes small enough for the triaxial torque to compensate for the positive secular torque at the later state, as suggested by Murray & Dermott (2000) for the Moon. Otherwise, the tidal despinning is arrested in the pseudosynchronous state. However, as was explained later by Makarov & Efroimsky (2013), this is merely a mathematical feature of the simplified linear model which is not consistent with the rheological properties of actual solids.

Within the constant time lag model employed by Correia & Laskar (2004), the rate of pseudosynchronous rotation depends on the eccentricity, wherefore a gradual increase of eccentricity allows the spin to reverse its trend and to cross the 3:2 spin-orbit resonance repeatedly. Using this mathematical feature, Correia & Laskar (2004) find a final probability of capture of 55.4%, 554 trajectories being eventually trapped. So this study identifies the chaotic evolution of the eccentricity of Mercury as the likely cause of its current rotational state, the core-mantle friction not being considered at that point.

To reproduce the results from Correia & Laskar (2004), we ran 10 sets of 1,000 simulations each, all starting with a spin period of 20 days. As stated in *Ibid.*, the choice of the initial spin rate is not critical, and high-order resonances are not likely to be important. For computational reasons, we integrated over only 3 Myr, which is long enough to slow down Mercury and to reach the Type I captures. Each set of 1,000 simulations uses the same set of 1,000 synthetic eccentricity trajectories, the differences between our 10 sets being only in the initial value of the sidereal angle θ . We use these 10 sets to check how the number of trapped trajectories can change from one set to another, with the same eccentricities.

The histogram of the final spin rates at the end of the 10,000 simulations is given in

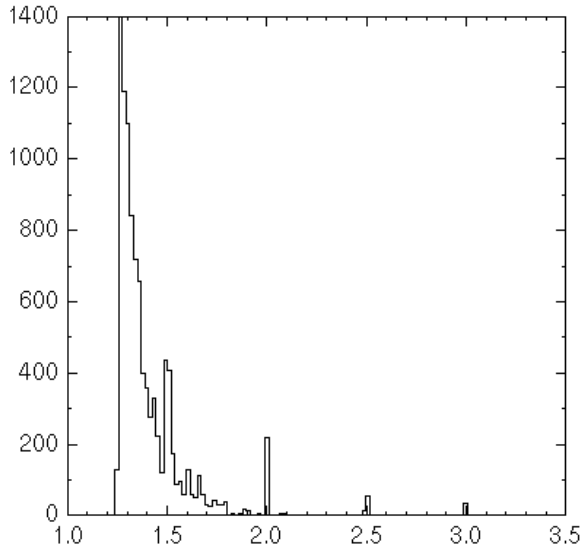


Fig. 8.— Histogram of the final spin rates $\dot{\theta}/n$ of our 10,000 simulations covering 3 Myr and based on the CTL tidal model.

Figure 8. We can see small peaks corresponding to the low-order spin-orbit resonances. The final spin rate always exceeds $1.2n$. The number of trajectories trapped into the 2:1, 5:2 and 3:1 resonances can be estimated from the plot. For the 3:2 resonance, however, some of the trajectories ending at this spin rate, may not be actually trapped, because the continuum distribution around 1.5 implies that some trajectories were simply caught by the end of integration while in fact traversing the resonance. For this reason, we fit a mathematical approximation to the continuum part of the histogram. Denoting with $f(\dot{\theta})$ the number of trajectories whose final spin rate is $\dot{\theta}$, we fit the function

$$f(\dot{\theta}) \approx \frac{a}{\dot{\theta}^b}, \quad (26)$$

and obtain: $a = 31,476.4 \pm 2,836$ and $b = 12.9944 \pm 0.3311$. Of course, these numbers depend on the size of the bin, which in our case was $0.0188n$. The equality $f(\dot{\theta}) = N$ means that there are N trajectories for which the final spin rate lies between $\dot{\theta} - 0.0094n$ and $\dot{\theta} + 0.0094n$.

Over 10,000 trajectories, we obtain:

- 577 trajectories close to the 3:2 resonance ($\dot{\theta}/n$ between 1.4906 and 1.5094),
- 221 trajectories close to the 2:1 resonance ($\dot{\theta}/n$ between 1.9906 and 2.0094),
- 70 trajectories close to the 5:2 resonance ($\dot{\theta}/n$ between 2.4906 and 2.5094),

- 35 trajectories close to the 3:1 resonance ($\dot{\theta}/n$ between 2.9906 and 3.0094),

With $f(1.5n) \approx 162.1007$, $f(2n) \approx 3.8573$, $f(2.5n) \approx 0.2123$, and $f(3n) \approx 0.0199$, our estimate tells us that we have 415 ($= 577 - f(1.5n)$) captures into the 3:2 resonance, 217 into the 2:1, 70 into the 5:2, and 35 into the 3:1 one. We use the function f rendered by the equation (26) to evaluate the number of resonant trajectories in each of our 10 sets of 1,000 simulations. The results are gathered in Table 3.

Table 3: Evaluation of the number of entrapments in the 10 sets of 1,000 numerical simulations. These numbers result from an estimate of the untrapped trajectories with the function f given by the equation (26). As a consequence of round-off errors, the *Total* row does not exactly correspond to the sum of the 10 sets.

	3:2	2:1	5:2	3:1
Set 0	37	20	8	5
Set 1	47	15	5	1
Set 2	51	22	10	4
Set 3	34	26	8	8
Set 4	56	21	5	1
Set 5	35	28	6	4
Set 6	40	23	6	1
Set 7	29	17	11	3
Set 8	39	26	5	7
Set 9	49	23	6	1
Total	415	217	70	35

We can see that the statistics significantly vary between our 10 sets, which is expected due to the Poisson distribution of the number of positive outcomes. We obtain between 29 and 56 Type I captures into the 3:2 resonance, while Correia & Laskar (2004) get 31. Thus, our results are consistent. We can now consider that our simulation methodology is valid and use it to check the influence of the tidal model.

7.3. Our method

In contradistinction to our predecessors, we rely on a description which combines a realistic rheology of the mantle with self-gravitation of the planet. Our starting point is the

afore-justified approximation (12b), i.e., the expression

$$\mathcal{T}_z^{(TIDE)} = \frac{3}{2} \frac{GM_{star}^2}{a} \left(\frac{R}{a}\right)^5 \sum_{q,j=-5}^5 G_{20q}(e) G_{20j}(e) k_2(\omega_{220q}) \sin |\epsilon_2(\omega_{220q})| \text{Sgn}(\omega_{220q}) \cos [(q-j)\mathcal{M}] + O(e^6\epsilon) + O(i^2\epsilon) + O((R/a)^7\epsilon) , \quad (27)$$

for the polar component of the tidal torque. Together with the expression (10) for the triaxiality-caused torque, the formula (27) is inserted into the law of motion (4).

The expression (27) contains the so-called quality function $k_l(\omega_{lmpq}) \sin \epsilon_l(\omega_{lmpq}) = k_l(\omega_{lmpq}) \sin |\epsilon_l(\omega_{lmpq})| \text{Sgn}(\omega_{lmpq})$ whose functional form is defined by the mantle rheology and by the self-gravitation of the planet. As explained in Appendix B, the absolute value of the quality function is calculated as

$$k_l(\omega_{lmpq}) \sin |\epsilon_l(\omega_{lmpq})| = -\frac{3}{2(l-1)} \frac{A_l \mathcal{I}}{(\mathcal{R} + A_l)^2 + \mathcal{I}^2} , \quad (28)$$

where \mathcal{R} and \mathcal{I} are the dimensionless real and imaginary parts of the complex compliance $\bar{J}(\chi)$ of the mantle:

$$\mathcal{R} = 1 + (\chi\tau_A)^{-\alpha} \cos\left(\frac{\alpha\pi}{2}\right) \Gamma(\alpha + 1) , \quad (29)$$

$$\mathcal{I} = -(\chi\tau_M)^{-1} - (\chi\tau_A)^{-\alpha} \sin\left(\frac{\alpha\pi}{2}\right) \Gamma(\alpha + 1) . \quad (30)$$

Here χ is a shortened notation for the physical forcing frequency

$$\chi_{lmpq} \equiv |\omega_{lmpq}| = |(l-2p+q)n - m\dot{\theta}| , \quad (31)$$

α is the Andrade parameter (about 0.2 for silicates with partial melt), while τ_M and τ_A are the Maxwell time and the Andrade time of the mantle. The auxiliary factors A_l entering (27) are furnished by

$$A_l = \frac{3\mu(2l^2 + 4l + 3)}{4l\pi G\rho^2 R^2} , \quad (32)$$

where μ , ρ and R are the unrelaxed rigidity, mean density and radius of the planet, while G is the Newton gravitational constant. Evidently, the presence of these factors is owed to the competition between rheology and self-gravitation (which, somewhat naïvely speaking, is playing the role of extra rigidity).

To avoid numerical complications in the zero-frequency limit (i.e., on crossing resonances), it is convenient to multiply both the numerator and denominator of (28) by χ :

$$k_l(\omega_{lmpq}) \sin |\epsilon_l(\omega_{lmpq})| = - \frac{3}{2(l-1)} \frac{A_l \mathcal{I}' \chi}{(\mathcal{R}' + A_l \chi)^2 + \mathcal{I}'^2}, \quad (33)$$

where

$$\mathcal{R}' = \chi + \chi^{1-\alpha} \tau_A^{-\alpha} \cos\left(\alpha \frac{\pi}{2}\right) \Gamma(\alpha + 1), \quad (34)$$

$$\mathcal{I}' = -\tau_M^{-1} - \chi^{1-\alpha} \tau_A^{-\alpha} \sin\left(\alpha \frac{\pi}{2}\right) \Gamma(\alpha + 1). \quad (35)$$

Numerical implementation of the tidal model (27) requires a much longer computation time than for the model (20). As a consequence, it is tempting to artificially accelerate the tidal dissipation, through multiplying the expression (27) by a constant factor. Based on the theory of adiabatic invariants (Henrard 1982), this procedure is widely employed in the studies of long-term orbital dynamics. The basic idea behind this procedure is that it artificially amplifies the action of tides, without altering the capture probabilities, provided that the tidal deceleration nevertheless remains *sufficiently slow*. The term *sufficiently slow* implies that the despinning time (15) remains much longer than the rotation period (Malhotra 1991). Using this trick, we first run a set of 1,000 simulations of the despinning of Mercury, with our synthetic eccentricities and with the tidal torque being 16 times larger than the actual value – see the subsection 8.1 below. Then we carried out 40 simulations of the *exact* differential equation where the tidal torque was *not* enhanced – see the subsection 8.2. Finally we run, for each of the most interesting 5 resonances (7:2, 3:1, 5:2, 2:1 and 3:2), a set of 1,000 simulations starting close to the resonance, to see whether the system is trapped or not – see the subsection 8.3.

8. Our results

This section presents the statistics of entrapment into spin-orbit resonances, based on the realistic tidal model, i.e., on the formula (27) wherein the tidal response (33 - 35) is plugged. Recall that the latter formulae reflect the inputs from both rheology and self-gravitation.

8.1. 1,000 artificially accelerated trajectories

The time span of each of our 1,000 accelerated simulations is 3 Myr. The tidal torque being enhanced by a factor of 16, this in fact is equivalent to simulation over 48 Myr. It

turns out that in practice the 3:2 resonance is often reached in 20 Myr.

The capture statistics are as follows:

- resonance 7:2 : 4 captures (0.4%),
- resonance 3:1 : 47 captures (4.7%),
- resonance 5:2 : 146 captures (14.6%),
- resonance 2:1 : 289 captures (28.9%),
- resonance 3:2 : 401 captures (40.1%),
- resonance 1:1 : 40 captures (4%).

The 73 remaining trajectories are between the 1:1 and the 3:2 resonance and are bound to be trapped in the synchronous resonance, as the secular tidal torque is negative (decelerating). The histogram of these trajectories is presented in Figure 9, to be compared with Figure 8.

We conclude, in particular, that the 3:2 resonance is the most probable for the Type I captures. Moreover, other types of captures are much less likely since the tidal despinning drives the spin rate to the synchronous rotation $\dot{\theta} = n$, making more than one crossing of the resonance impossible. As the evolution of the eccentricity will not change these results of resonant trapping, we can safely avoid the necessity to numerically integrate the spin evolution further in time.

8.2. Some unaccelerated trajectories

In order to check the reliability of accelerating the tides 16 times, we ran 40 trajectories where the tides are not accelerated. The results are:

- resonance 7:2 : 0 capture (0%),
- resonance 3:1 : 1 capture (2.5%),
- resonance 5:2 : 3 captures (7.5%),
- resonance 2:1 : 9 captures (22.5%),

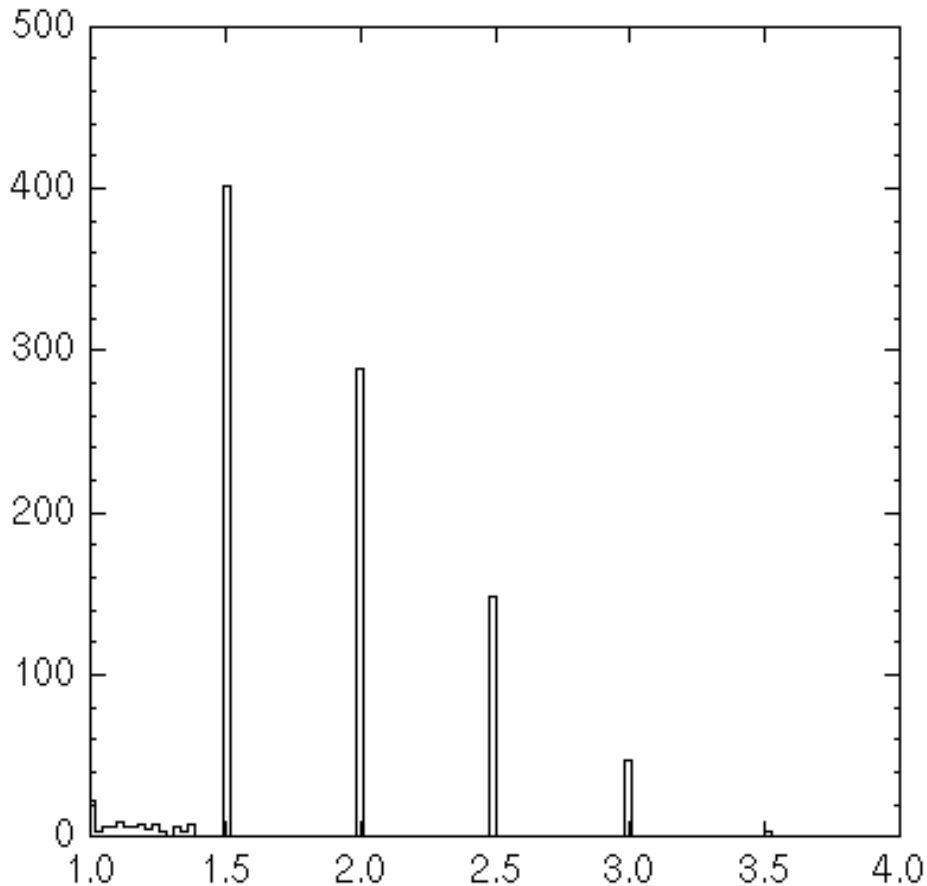


Fig. 9.— Distribution of the final spin rates of our 1,000 trajectories integrated with the secular USNO model (27 - 28), the tides being accelerated 16 times. It can be seen that the 3 : 2 resonance is the most probable destination, contrarily to the result of Correia & Laskar (2004) who relied on the commonly used CTL tidal model.

- resonance 3:2 : 24 captures (60%),
- resonance 1:1 : 3 captures (7.5%).

Once again, the 3:2 spin-orbit resonance is the most probable final destination. However, we should be careful with the statistics extracted from such a small set of data, i.e., from only 40 trajectories. For this reason, another set of 1,000 simulations for each resonance has been investigated, each beginning just above the resonant points.

8.3. Dynamics near the resonances

We run our simulations starting with $\dot{\theta}$ slightly above the resonant value. This allows us to save on the computing time, while not boosting the tidal acceleration. We also make the assumption that the eccentricities (taken from the 1,000 synthetic orbits at $T = -4$ Gyr) remain constant during the short interval of integration. Overall, we generated 5 sets of 1,000 simulations, each set corresponding to one of the resonances (7:2, 3:1, 5:2, 2:1 and 3:2), and with the tides not accelerated. This outcome is as follows:

- Resonance 7:2 : 25 captures ,
- Resonance 3:1 : 53 captures ,
- Resonance 5:2 : 165 captures ,
- Resonance 2:1 : 462 captures ,
- Resonance 3:2 : 884 captures .

To interpret the results of these localised integrations, in the light of the previously-performed long-term runs, we would first emphasise a crucial feature demonstrated by our numerics: *a capture of Mercury cannot be temporary*. All our integration runs, long- or short-term, confirm this unequivocally: as soon as Mercury is trapped into a certain spin-orbit resonance, it never jumps out. Even if escapes are possible, they must be extremely rare; and we never managed to observe one. To understand the reason for this confinement, recall that the only route to escape lies through a major increase of the magnitude of the forced librations. Such increase may indeed take place when the eccentricity of a locked planet is pumped up by the gravitational pool of its fellow planets. At the same time, though, the amplitude of the secular tidal kink will be growing too, mitigating libration and thus preventing escape. This competition is a subtle issue, altogether; and we cannot exclude the possibility of escape for very elongated celestial bodies. For Mercury, however, the probability of such an event is low, if not zero. As a result of this, the point probabilities on the above list should be replaced with the cumulative probabilities:

- Resonance 7:2 : 25 captures (2.5%) ,
- Resonance 3:1 : 53 captures, though only $975 = 1000 - 25$ histories had a chance to reach this resonance, so the probability is $P_{3:1} = 53/1000 \times 975/1000 = 5.2\%$,

- Resonance 5:2 : 165 captures while $923 = 1000 - 25 - 52$ trajectories can reach it, so $P_{5:2} = 15.2\%$,
- Resonance 2:1 : 462 captures while $768 = 1000 - 25 - 52 - 152$ trajectories can reach it, so $P_{2:1} = 35.6\%$,
- Resonance 3:2 : 884 captures while $406 = 1000 - 25 - 52 - 152 - 356$ trajectories can reach it, so $P_{3:2} = 36.7\%$,

the remaining trajectories being bound to fall into the 1:1 resonance ($P_{1:1} = 4.8\%$). We can see that, once again, the 3:2 resonance is the most frequent end-state. These numbers can be compared to the ones of Subsection 8.1. For the resonance 3:2, the probability of capture seems to be almost the same, but it seems to be higher for the 2:1 resonance. Anyhow, the 3:2 resonance remains the most probable.

The Figure 10 illustrates a correlation between the final spin rate and the eccentricity for the resonances 2:1 and 3:2. We can see a clear connection between these two quantities. In particular, the 3:2 resonance is a certain end-state for $e > 0.2$, and 2:1 is for $e > 0.32$. This is consistent with Makarov (2012).

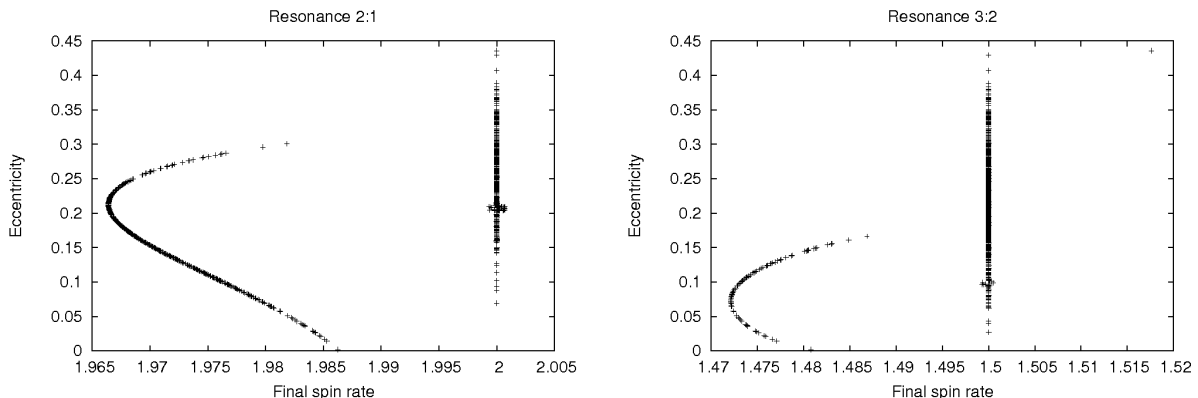


Fig. 10.— The final rotation state rendered by our simulations, with the unaccelerated tidal model (27 - 28). The simulations start from the right, i.e. from a slightly higher spin rate, and follow the slow-down of Mercury.

9. Discussion

In the article thus far, we investigated the process of tidal despinning of Mercury, from faster prograde spin rates down to entrapment in a spin-orbit resonance. Numerical integra-

tion of several thousand trajectories differing in the initial conditions has furnished us the probabilities of capture into most prominent resonances. It has turned out that the capture probabilities depend greatly upon the tidal model employed. Such a strong dependence has already been hinted by several authors, e.g., Goldreich & Peale (1966), Makarov (2012). We confirm this dependence for the case of Mercury, with extensive and accurate numerical simulations which take into account the chaotic variations of its eccentricity.

The main result of our study is that the 3:2 resonance is the most probable end state of tidal evolution, if the initial spin rate was prograde and fast. When such trapping occurs, it does so during the first crossing of the resonance, our tidal model preventing further releases or additional crossings. Such trappings are called *Type I captures*, and they are the only trappings possible. This is the first drastic difference between our model and that employed in the paper by Correia & Laskar (2004), where numerous crossings of the 3:2 resonance were possible (and were needed to ensure a sufficiently high probability of this resonance as the end state).

Another crucial difference is that within our tidal model captures into the 3:2 spin-orbit resonance usually they happen in less than 20 Myr, while in the scenario of Correia & Laskar (2004) entrapment could take up to 1 Gyr. Since our modeling was based on a realistic rheological model, the swift capture obtained by us means that the current 3:2 spin-orbit resonance could be much older than expected. With a characteristic despinning time less than 10^8 yr, Mercury has been, in all likelihood, residing in the present-day 3:2 resonance for billions of years. This may have some interesting physical consequences for the tidal heating history of Mercury, the origin of its shape features, and its massive molten core.

A further step along this line of research could be exploring the influence of the core-mantle friction on the despinning of Mercury. Several authors have shown that this friction is capable of enhancing the capture process (Peale & Boss 1977, Correia & Laskar 2009). If, within a plausible range of physical parameters, trapping of a so-stratified Mercury into the 2:1 resonance becomes certain, this will indicate that stratification took place *after* the capture into the 3:2 resonant state. In other words, this would be an extra confirmation of the afore-stated result that the said capture took place at a very early stage of Mercury's history (provided the initial spin was prograde).

Acknowledgements

Benoît Noyelles is an F.R.S.-FNRS post-doctoral research fellow, and he thanks this institution for having funded two of his visits to the US Naval Observatory. This research

made use of the resources of the Interuniversity Scientific Computing Facility located at the University of Namur, Belgium, which is supported by the F.R.S.-FNRS under Convention No. 2.4617.07. Julien Frouard is an UNESP post-doctoral research fellow (Process No. 2010/52715-5). The authors are indebted to Valéry Lainey and Christophe Le Poncin-Lafitte who made this collaboration possible by putting them in touch.

Appendix

A. Expression for the tidal torque

A.1. Fourier tidal modes

The additional tidal potential U of a tidally disturbed homogeneous sphere can be expanded into a Fourier series over the modes

$$\omega_{lmpq} \equiv (l - 2p) \dot{\omega} + (l - 2p + q) \dot{\mathcal{M}} + m (\dot{\Omega} - \dot{\theta}) \approx (l - 2p + q) n - m \dot{\theta} . \quad (\text{A1})$$

where the notations θ and $\dot{\theta}$ stand for the sidereal angle and spin rate of the perturbed spherical body; while ω , Ω , n , and \mathcal{M} are the pericentre, the node, the mean motion, and the mean anomaly of the perturber as seen from the perturbed body. While the tidal modes ω_{lmpq} can assume either sign, the physical forcing frequencies

$$\chi_{lmpq} = |\omega_{lmpq}| \approx |(l - 2p + q) n - m \dot{\theta}| , \quad (\text{A2})$$

at which the tidal strain and stress are evolving, are positive-definite.

Derivation of a partial sum of the series was pioneered by Darwin (1879),⁸ the full series worked out in Kaula (1964). Extended presentation of this formalism, with historical notes and explanation of some details omitted by Kaula (1964), is offered in Efroimsky & Makarov (2013).

A.2. Expansion of the tidal torque

A Fourier expansion of the tidally generated torque was written down, without proof, by Goldreich & Peale (1966) who took into account only the secular part of the torque. Later, a

⁸ In the modern notation, Darwin's treatment is discussed by Ferraz-Mello et al. (2008).

schematic derivation of their formula was offered by Dobrovolskis (2007). A comprehensive derivation of the polar component of the torque can be found in Efroimsky (2012a) where it is demonstrated that the torque contains both a secular and a rapidly oscillating part. The overall expression reads as

$$\begin{aligned} \mathcal{T}_z^{(TIDE)} = & - \sum_{l=2}^{\infty} \left(\frac{R}{a} \right)^{2l+1} \frac{G M_{star}^2}{a} \sum_{m=1}^l \frac{(l-m)!}{(l+m)!} 2 m \sum_{p=0}^l F_{lmp}(i) \sum_{q=-\infty}^{\infty} G_{lpq}(e) \\ & \sum_{h=0}^l F_{lmh}(i) \sum_{j=-\infty}^{\infty} G_{lhj}(e) k_l \sin [v_{lmpq} - v_{lmhj} - \epsilon_l] , \end{aligned} \quad (\text{A3})$$

where ϵ_l are the phase lags, G stands for the Newton gravitational constant, while $F_{lmp}(i)$ and $G_{lhj}(e)$ denote the inclination functions and eccentricity polynomials. The auxiliary quantities v_{lmpq} are rendered by

$$v_{lmpq} \equiv (l - 2p) \omega + (l - 2p + q) \mathcal{M} + m \Omega , \quad (\text{A4})$$

where $a, e, i, \omega, \Omega, \mathcal{M}$ stand for the orbital elements of the perturbing secondary, as seen in the reference frame associated with the equator of the perturbed primary. While the frame may precess with the primary's equator, it does *not* corotate with it.

In our situation, the role of the primary is played by the planet, its host star being regarded as the secondary. This means that the apparent inclination i of the secondary (the star) on the equator of the primary (the planet) will in fact be the planet's obliquity. This also means that the mass of the secondary, M_{star} , is to be the mass of the star.

The expression (A3) furnishes the tidal torque's projection onto the spin axis of the perturbed body. Taking into account this component solely, we neglect the planet's precession. This approach is acceptable when the inclination (in our case, obliquity) i is small.

As explained in detail in Efroimsky (2012a,b), expression (A3) is obtained from the Darwin-Kaula expansion of the tidal potential, through differentiation thereof with respect to the negative sidereal angle θ , which enters the $lmpq$ term of the expansion as $m\theta$. Differentiation inserts the multiplier m into each term, as we see in (A4). This way, while in the expansion for the potential the summation over m goes from $m = 0$, in the expansion for torque we sum beginning with $m = 1$.

A.3. The tidal lags

The Fourier tidal modes ω_{lmpq} emerging in the Darwin-Kaula theory are given by (A1), while the positive-definite actual frequencies χ_{lmpq} excited by the tides are rendered by

(A2). The corresponding positive-definite time delays $\Delta t_l(\chi_{lmpq})$ depend on this physical frequency, the functional forms of this dependence being different for different materials.

As demonstrated, e.g., in Efroimsky & Makarov (2013), within the Darwin-Kaula theory the phase lags emerge as the products of the Fourier modes ω_{lmpq} by the time lags which themselves are frequency-dependent:⁹

$$\epsilon_l(\omega_{lmpq}) = \omega_{lmpq} \Delta t_l(\chi_{lmpq}) = \pm \chi_{lmpq} \Delta t_{lmpq} , \quad (\text{A5a})$$

Owing to causality, time lags $\Delta t_l(\chi_{lmpq})$ are positive-definite, so the lags (A5a) become

$$\epsilon_l(\omega_{lmpq}) = \chi_{lmpq} \Delta t_l(\chi_{lmpq}) \text{Sgn}(\omega_{lmpq}) , \quad (\text{A5b})$$

where χ_{lmpq} are the forcing frequencies (A2).

In neglect of the apsidal and nodal precession and also of $\dot{\mathcal{M}}_0$, the expressions for the frequencies and lags can be approximated with:¹⁰

$$\omega_{lmpq} = (l - 2p + q)n - m\dot{\theta} , \quad (\text{A6})$$

$$\chi_{lmpq} \equiv |\omega_{lmpq}| = |(l - 2p + q)n - m\dot{\theta}| , \quad (\text{A7})$$

and

$$\epsilon_l(\omega_{lmpq}) = \chi_{lmpq} \Delta t_l(\chi_{lmpq}) \text{Sgn} \left[(l - 2p + q)n - m\dot{\theta} \right] , \quad (\text{A8})$$

⁹ Just as the Love numbers $k_l(\omega_{lmpq})$, so the lags are written down as $\epsilon_l(\omega_{lmpq})$ and $\Delta t_l(\chi_{lmpq})$ – and not as ϵ_{lmpq} and Δt_{lmpq} . This uniformity of nomenclature is needed to emphasise that for a homogeneous spherical body the functional forms of the lags and Love numbers (as functions of the Fourier mode) are determined only by the degree l . The dependence of $k_l(\omega_{lmpq})$, $\epsilon_l(\omega_{lmpq})$ and $\Delta t_l(\chi_{lmpq})$ upon m, p, q comes into being only due to the m, p, q -dependence of the arguments ω_{lmpq} and χ_{lmpq} .

This however applies to spherical homogeneous objects only. For nonspherical bodies, the functional form of the lags and Love numbers acquires dependence also on integers other than the degree. For a symmetrical oblate body, the lags and Love numbers will depend also upon the order m . Accordingly, our notations $k_l(\omega_{lmpq})$, $\epsilon_l(\omega_{lmpq})$, $\Delta t_l(\chi_{lmpq})$ will have to be changed to $k_{lm}(\omega_{lmpq})$, $\epsilon_{lm}(\omega_{lmpq})$, $\Delta t_{lm}(\chi_{lmpq})$. For a slightly non-spherical body, the Love numbers and lags differ from the Love numbers and lags of the spherical reference body by terms of the order of the flattening, so a small non-sphericity can be neglected.

¹⁰ Generally, the mean anomaly of the perturber is equal to $\mathcal{M} = \mathcal{M}_0 + \int_{t_0}^t n(t) dt$, where $n(t) \equiv \sqrt{G(M_{star} + M_{planet})} a^{-3/2}(t)$. This yields: $\dot{\mathcal{M}} = \dot{\mathcal{M}}_0 + n \approx n$. The term $\dot{\mathcal{M}}_0$ comes into play when the orbital motion is disturbed by exterior influences (say, the pull of the third body). Note that in this present study, we use a secular value of n (see Table 2) which already takes into account these exterior perturbations.

$\dot{\theta}$ being the sidereal spin rate of the perturbed body.

Importantly, the Darwin-Kaula formalism and the ensuing expression for the torque impose no *a priori* constraint on the form of frequency-dependence of the lags.¹¹

A.4. Simplification 1: algebraic development

Numerical approximation of the series (A3) is not easy because of the summation over six indices. Fortunately, much of the work can be performed analytically, the numerical part of the work thus being reduced to the necessary minimum. In this subsection, we shall simplify the expansion analytically, and in the subsequent subsections shall truncate the series to a partial sum.

From (A4), we see that

$$\begin{aligned} v_{lmpq} - v_{lmhj} &= [(l - 2p)\omega + (l - 2p + q)\mathcal{M} + m\Omega] - [(l - 2h)\omega + (l - 2h + j)\mathcal{M} + m\Omega] \\ &= 2(h - p)(\omega + \mathcal{M}) + (q - j)\mathcal{M} \quad , \end{aligned} \quad (\text{A9})$$

insertion whereof into (A3) makes the latter look as

$$\begin{aligned} \mathcal{T}_z^{(TIDE)} &= - \sum_{l=2}^{\infty} \left(\frac{R}{a}\right)^{2l+1} \frac{GM_{star}^2}{a} \sum_{m=1}^l \frac{(l-m)!}{(l+m)!} 2m \sum_{p=0}^l F_{lmp}(i) \sum_{q=-\infty}^{\infty} G_{lpq}(e) \\ &\quad \sum_{h=0}^l F_{lmh}(i) \sum_{j=-\infty}^{\infty} G_{lhj}(e) k_l \sin [2(h-p)(\omega + \mathcal{M}) + (q-j)\mathcal{M} - \epsilon_l] \quad . \end{aligned} \quad (\text{A10})$$

If we expand each sine as

$$\sin [2(h-p)(\omega + \mathcal{M}) + (q-j)\mathcal{M}] \cos \epsilon_l - \cos [2(h-p)(\omega + \mathcal{M}) + (q-j)\mathcal{M}] \sin \epsilon_l \quad (\text{A11})$$

¹¹ The MacDonald (1964) theory of tides imposes implicitly a particular dissipation law (Williams & Efroimsky 2012, Efroimsky & Makarov 2013). In his work, MacDonald (1964) did not notice this, and erroneously set the dissipation quality factor to be frequency-independent, which was in contradiction with the pre-imposed dissipation law. Later, his theory was corrected by Singer (1968) and Mignard (1979, 1980). Although compact and elegant, the so-corrected version of MacDonald's theory still has no practical application, because the dissipation law, whereon it relies, differs considerably from the rheology of realistic minerals (Efroimsky & Lainey 2007).

and recall that $\cos \epsilon \approx 1 + O(\epsilon^2)$, all the terms with $\sin [(q - j) \mathcal{M}]$ will cancel, in the order of $O(\epsilon^2)$, after the summation over both q and j is performed. This will leave us with

$$\begin{aligned} \mathcal{T}_z^{(TIDE)} = & \sum_{l=2}^{\infty} \left(\frac{R}{a}\right)^{2l+1} \frac{G M_{star}^2}{a} \sum_{m=1}^l \frac{(l-m)!}{(l+m)!} 2 m \sum_{p=0}^l F_{lmp}(i) \sum_{q=-\infty}^{\infty} G_{lpq}(e) \\ & \sum_{h=0}^l F_{lmh}(i) \sum_{j=-\infty}^{\infty} G_{lhj}(e) k_l \sin \epsilon_l \cos [2 (h - p) (\omega + \mathcal{M}) + (q - j) \mathcal{M}] . \end{aligned} \quad (\text{A12})$$

In the literature, it is customary to consider only the terms with $h = p$, $q = j$, i.e., with $\cos [2 (h - p) (\omega + \mathcal{M}) + (q - j) \mathcal{M}] = 1$. The reason for this is that for $h \neq p$ or/and $q \neq j$ the cosine averages out to nil,¹² wherefore the oscillating terms vanish *in average*. This leaves one with the secular part of the torque.

As explained in Efroimsky (2012), there exists a reason why the oscillating part of the torque may influence the process of entrapment into resonances. The frequencies $n(2h - 2p + q - j)$, which show up in the oscillating part of the torque, are integers of n , and thus become commensurate with the spin rate $\dot{\theta}$ near resonances. It indeed was discovered, via numerical modeling, that the presence of the oscillating part changes histories. Whether a history stemming from a particular set of initial conditions leads to entrapment or to transition – that is influenced by the presence or absence of the oscillating part of the torque. The resulting statistics, though, remains virtually unchanged (Makarov et al. 2012). Just in case, we here shall include the oscillating part into computation.

A.5. Simplification 2: approximation of the series with its quadrupole part

We shall approximate the polar torque with the $l = 2$ input:

$$\mathcal{T}_z^{(TIDE)} = {}^{(l=2)}\mathcal{T}_z^{(TIDE)} + O\left(\left(\frac{R}{a}\right)^7 \epsilon\right) = {}^{(lm=21)}\mathcal{T}_z^{(TIDE)} + {}^{(lm=22)}\mathcal{T}_z^{(TIDE)} + O\left(\left(\frac{R}{a}\right)^7 \epsilon\right) , \quad (\text{A13})$$

where the $l = 2$ input is of the order of $(R/a)^5 \epsilon$, while the $l = 3, 4, \dots$ inputs constitute $O\left(\left(\frac{R}{a}\right)^7 \epsilon\right)$. As ever, R and a denote the planet’s radius and semimajor axis, while ϵ stands for the phase lag. The index m runs through the values¹³ from 1 through $l = 2$.

¹² The averaging period should be the period of apparent rotation of the perturber about the perturbed body. In our case, it is the synodal day of the planet.

¹³ Recall that, while the $m = 0$ terms enter the potential, they add nothing to the torque, because m enters (A10) as a multiplier.

In a comprehensive form, (A13) reads as

$$\begin{aligned} \mathcal{T}_z^{(TIDE)} = & \left(\frac{R}{a}\right)^5 \frac{G M_{star}^2}{a} \sum_{m=1}^2 \frac{(2-m)!}{(2+m)!} 2 m \sum_{p=0}^2 F_{2mp}(i) \sum_{q=-\infty}^{\infty} G_{2pq}(e) \sum_{h=0}^2 F_{2mh}(i) \\ & \sum_{j=-\infty}^{\infty} G_{2hj}(e) k_2 \sin \epsilon_2 \cos [2(h-p)(\omega + \mathcal{M}) + (q-j)\mathcal{M}] + O(\epsilon(R/a)^7) \quad , \quad (A14) \end{aligned}$$

A.6. Simplification 3: diagonalisation over the indices p and h

Above we mentioned that our formulae for the tidal torque furnish the torque's component along the spin axis of the perturbed body. This component is sufficient when the inclination of the perturber, i , is small. When the role of a tidally disturbed primary is played by a planet and the role of the perturber is played by the host star, the apparent inclination coincides with the planet's obliquity which, for Mercury, is $i = 2.04 \pm 0.08$ arcmin (Margot et al. 2012). This enables us to make a further simplification of the formula for the torque, truncating away the terms of the order of $O(i^2)$.

To this end, we should notice that, among the terms with $l = 2$, we should keep only those containing the inclination functions with subscripts $(lmp) = (220), (210), (211)$:

$$F_{220}(i) = 3 + O(i^2) \quad , \quad F_{210}(i) = \frac{3}{2} \sin i + O(i^2) \quad , \quad F_{211}(i) = -\frac{3}{2} \sin i + O(i^2) \quad , \quad (A15)$$

all the other $F_{2mp}(i)$ being of order $O(i^2)$ or higher. As the inclination functions enter the expansion in combinations $F_{lmp}(i) F_{lmh}(i)$, we see that it is sufficient, in the $O(i^2)$ approximation, to take into account only the terms with $F_{220}^2(i)$, ignoring those containing $F_{210}^2(i)$, $F_{211}^2(i)$, or $F_{210}(i) F_{211}(i)$. Thus the $l = 2$ input into the torque gets simplified to:

$$\mathcal{T}_z^{(TIDE)} = {}^{(l=2)} \mathcal{T}_z^{(TIDE)} + O((R/a)^7 \epsilon) = {}^{(lmp=2200)} \mathcal{T}_z^{(TIDE)} + O(i^2 \epsilon) + O((R/a)^7 \epsilon) = \quad (A16)$$

$$\frac{3}{2} \frac{G M_{star}^2}{a} \left(\frac{R}{a}\right)^5 \sum_{q=-\infty}^{\infty} G_{20q}(e) \sum_{j=-\infty}^{\infty} G_{20j}(e) k_2 \sin \epsilon_2 \cos [(q-j)\mathcal{M}] + O(i^2 \epsilon) + O((R/a)^7 \epsilon) \quad ,$$

where the absolute error $O(i^2 \epsilon)$ comes into being after the neglect of terms with $p, h \geq 1$.

A.7. Simplification 4: truncation over the indices q and j

In our numerical simulations, the eccentricity of Mercury never exceeded $e = 0.45$. Moreover, it exceeded $e = 0.4$ in several isolated cases and for only short time spans. In

neglect of these unique episodes, we may assume that the eccentricity stays lower than 0.4.

The question then becomes how many terms of the series (A16) should be taken into consideration. The issue is nontrivial, because the higher the eccentricity the slower the convergence of the series. On the one hand, $|G_{lpq}(e)| = O(e^{|q|})$, which means that, in the leading order, $|G_{lpq}(e)| = A_{lpq} e^{|q|} + O(e^{|q|+1})$, with A_{lpq} being real numbers. On the other hand, the numbers A_{lpq} are growing rapidly with the increase of $|q|$, so the product $A_{lpq} e^{|q|}$ does not go immediately into decrease with an increasing $|q|$. For example, $G_{206}(0.4) = 0.25$, a significantly large value. Thence, for higher values of the eccentricity e , one needs to go to larger $|q|$, to make sure that the factor $e^{|q|}$ is small enough to keep the value of $A_{lpq} e^{|q|}$ lower than the needed precision level.

Apart from the eccentricity polynomials, a $2mpq$ term of the series (A16) includes the multiplier $k_2 \sin \epsilon_2$ which is a function of the Fourier tidal mode ω_{2mpq} . Therefore, to decide on how many terms should be kept in the series (A16), we should know the shape and magnitude of the so-called *quality function*

$$k_2 \sin \epsilon_2 = k_2(\omega_{2mpq}) \sin \epsilon_2(\omega_{2mpq}) = k_2(\omega_{2mpq}) \sin |\epsilon_2(\omega_{2mpq})| \text{Sgn}(\omega_{2mpq}) . \quad (\text{A17a})$$

For an arbitrary degree l , the appropriate quality functions would, of course, look:

$$k_l \sin \epsilon_l = k_l(\omega_{lmpq}) \sin \epsilon_l(\omega_{lmpq}) = k_l(\omega_{lmpq}) \sin |\epsilon_l(\omega_{lmpq})| \text{Sgn}(\omega_{lmpq}) . \quad (\text{A17b})$$

As will be explained in Appendix B below, for realistic terrestrial bodies the quality function has the shape of a kink centered at the point $\omega_{lmpq} = 0$, see Figure 2.

Inserting into (A17) the expression (A1) for the Fourier mode, we present the multiplier $k_2 \sin \epsilon_2$ as a function of the spin rate $\dot{\theta}$ of the tidally perturbed body:

$$k_2 \sin \epsilon_2 = k_2((2 - 2p + q)n - m\dot{\theta}) \sin \epsilon_2((2 - 2p + q)n - m\dot{\theta}) . \quad (\text{A18a})$$

For an arbitrary degree l , that would be:

$$k_l \sin \epsilon_l = k_l((l - 2p + q)n - m\dot{\theta}) \sin \epsilon_l((l - 2p + q)n - m\dot{\theta}) . \quad (\text{A18b})$$

It should be emphasised that here $((l - 2p + q)n - m\dot{\theta})$ denotes functional dependence on the argument $(l - 2p + q)n - m\dot{\theta}$, not multiplication by a factor of $(l - 2p + q)n - m\dot{\theta}$. The resulting functions of $\dot{\theta}$ will have a kink shape too, though the kink will now be centered around the point $\dot{\theta} = n(l - 2p + q)/m$ corresponding to $\omega_{lmpq} = 0$. Summation over the indices will yield a superposition of kinks, as in Figure 3. Be mindful that we now say *functions* and not *function*, because for different sets of the integers m, p, q we indeed

obtain different functional dependencies of $k_l \sin \epsilon_l$ upon $\dot{\theta}$. The numerical values of these functions are small everywhere except in close vicinities of resonances, i.e., of the aforementioned points $\dot{\theta} = n(l - 2p + q)/m$.

In our study, we limit ourselves to the degree $l = 2$. Moreover, as was demonstrated in subsection A.6 above, in the order $O(i^2)$ it is sufficient to take into account only the terms with $\{mp\} = \{20\}$ in the expression (A16) for the solar torque. So we shall be interested only in the dependencies

$$k_2 \sin \epsilon_2 = k_2(\omega_{220q}) \sin \epsilon_2(\omega_{220q}) = k_2((2 + q)n - 2\dot{\theta}) \sin \epsilon_2((2 + q)n - 2\dot{\theta}) . \quad (\text{A19})$$

It would not hurt to reiterate that $((2 - 2p + q)n - m\dot{\theta})$ denotes functional dependence on the argument $(2 - 2p + q)n - m\dot{\theta}$, not multiplication by a factor of $(2 - 2p + q)n - m\dot{\theta}$.

The functions (A19) will be peaked at $\dot{\theta} = n(l - 2p + q)/m = n(2 - q)/2$. For example, the terms with $q = 6$ will peak at the 4:1 resonance, i.e., when $\dot{\theta}/n = 4$.

Figure 11 demonstrates several contributions into the secular ($j = q$) part of the torque (A16). These are the contributions from the terms with $\{lmp\} = \{220\}$, $j = q$, calculated for the eccentricity value $e = 0.32$, for several values of q . Each contribution is rendered by the decimal logarithm of the absolute value of the angular acceleration caused by the appropriate input into the secular part of the torque. It can be understood from these plots that, unless we are interested in the passage through higher spin-orbit resonances, the terms with $|q|, |j| > 5$ can be omitted. Indeed, their input into the secular tidal torque is significantly smaller than that of the terms with $0 \leq |q| \leq 5$, even for the high value 0.32 of Mercury's eccentricity, which is close to the upper boundary of our range. Thus the simulations presented in this paper included the terms with $-5 \leq q \leq 5$ (though the terms with $-1 \leq q \leq 5$ would be sufficient to render virtually the same precision). Our choice limits the Taylor expansions of eccentricity-dependent functions to terms of the orders up to e^5 , inclusive. In our simulations, this truncation also precludes the possibility of capture into a resonance higher than 7:2. We found that a capture into the 7:2 resonance took place so rarely, that the omission of the remote possibility of capture into the 4:1, or higher, resonances does not alter our results appreciably. The resulting relative precision of our calculations is in most cases better than 1%, because the largest omitted term, the one with $q = 6$, is 0.009 times the largest included terms with $\dot{\theta} = \pi n$. For eccentricity values lower than the one used to generate these plots ($e = 0.32$), the relative precision of our calculations is much better, and it degrades rapidly towards the upper-limit eccentricities.

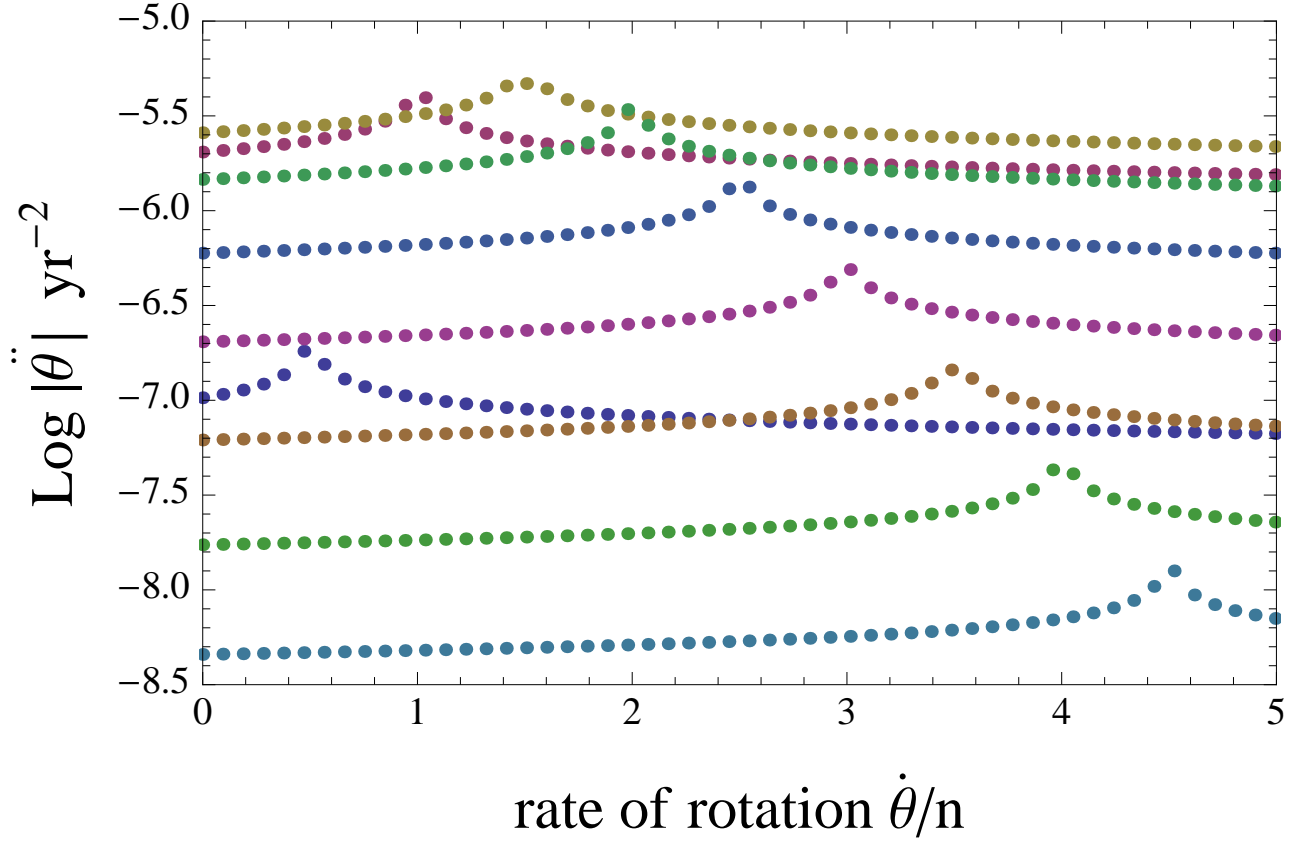


Fig. 11.— Contributions into the angular acceleration caused by the secular part of the tidal torque acting on Mercury. Curves on the plot depict the contributions from terms with $q = -1, 0, \dots, 7$. A curve corresponding to the q^{th} term can be identified by its peak located at $\dot{\theta}/n = (2+q)/2$. The plot is built for $e = 0.32$, which is close to the upper limit on eccentricity in our simulation. Be mindful that for this value of eccentricity the $q = 0$ term is superseded by two of the higher-order terms (those with $q = 1, 2$).

Thus we arrive at

$$\mathcal{T}_z^{(TIDE)} = \frac{3}{2} \frac{GM_{star}^2}{a} \left(\frac{R}{a}\right)^5 \sum_{q,j=-5}^5 G_{20q}(e) G_{20j}(e) k_2 \sin \epsilon_2 \cos [(q-j) \mathcal{M}] + O(e^6 \epsilon) + O(i^2 \epsilon) + O\left(\left(\frac{R}{a}\right)^7 \epsilon\right), \quad (\text{A20})$$

the additional absolute error $O\left(\left(\frac{R}{a}\right)^7 \epsilon\right)$ originating from our neglect of terms with $|q|, |j| > 5$. In the sum (A20), the terms with $q = j$ constitute the secular part, the other terms being oscillating.

We would finally mention that in reality the terms with $q = -2$ and $j = -2$ fall out, because the numerical factors accompanying these terms happen to vanish identically. Another interesting observation is that the terms with $q, j = -5$ through $q, j = -3$ are accompanied with extremely small numerical factors and are inessential. So summation from -1 through 5 would be equally good.

A.8. The secular part of the torque

While the secular part of the total torque (A10) reads as

$$\langle \mathcal{T}_z^{(TIDE)} \rangle = \sum_{l=2}^{\infty} \left(\frac{R}{a}\right)^{2l+1} \frac{GM_{star}^2}{a} \sum_{m=1}^l \frac{(l-m)!}{(l+m)!} 2m \sum_{p=0}^l F_{lmp}^2(i) \sum_{q=-\infty}^{\infty} G_{lpq}^2(e) k_l \sin \epsilon_l, \quad (\text{A21a})$$

the secular part of the truncated version (A20) assumes the form of

$$\langle \mathcal{T}_z^{(TIDE)} \rangle_{l=2} = \frac{3}{2} GM_{star}^2 R^5 a^{-6} \sum_{q=-5}^5 G_{20q}^2(e) k_2 \sin \epsilon_2 + O(e^8 \epsilon) + O(i^2 \epsilon). \quad (\text{A21b})$$

In our computations, however, we employed the expression (A20), with the oscillating terms included.

B. How rheology and self-gravitation define the shape of the quality functions $k_l(\omega_{lmpq}) \sin \epsilon_l(\omega_{lmpq})$

An $lmpq$ term in the expansion of the tidal torque is proportional to a factor $k_l \sin \epsilon_l = k_l(\omega_{lmpq}) \sin \epsilon_l(\omega_{lmpq})$ which is a function of the Fourier mode ω_{lmpq} and goes under the

name of a¹⁴ quality function. The shapes of the quality functions are determined by the interplay of the planet’s rheology and self-gravitation. So one should expect that these functional dependencies will include, as parameters, the rheological constants of the mantle and also the density and radius of the planet.

In our previous works (Efroimsky 2012a,b), the topic was explored in detail for a homogeneous near-spherical body. It was demonstrated how the quality functions are expressed through the real and imaginary parts of the complex compliance of the mantle material and the planet’s radius and mass. The quality functions turned out to be odd. Although slightly different for different values of the degree l , the quality functions demonstrate similarity of shape and always look like a kink – see Figure 2.¹⁵ Each function $k_l(\omega_{lmpq}) \sin \epsilon_l(\omega_{lmpq})$ looks as a kink centered around the resonant point $\omega_{lmpq} = 0$. This way, an $lmpq$ term of the torque changes its sign when the appropriate commensurability is transcended.

Being odd, the quality functions can be rewritten as $k_l(\omega_{lmpq}) \sin |\epsilon_l(\omega_{lmpq})| \text{Sgn}(\omega_{lmpq})$, where the products $k_l(\omega_{lmpq}) \sin |\epsilon_l(\omega_{lmpq})|$ are even functions of the Fourier modes and therefore can be regarded as functions not of the tidal mode ω_{lmpq} but of its absolute value $\chi_{lmpq} = |\omega_{lmpq}|$, which is the actual physical frequency of the tidally induced stress:

$$\begin{aligned} k_l(\omega_{lmpq}) \sin \epsilon_l(\omega_{lmpq}) &= k_l(\omega_{lmpq}) \sin |\epsilon_l(\omega_{lmpq})| \text{Sgn}(\omega_{lmpq}) \\ &= k_l(\chi_{lmpq}) \sin |\epsilon_l(\chi_{lmpq})| \text{Sgn}(\omega_{lmpq}) . \end{aligned} \quad (\text{B1})$$

As was shown in *Ibid.*, the quality functions have the form

$$k_l(\omega_{lmpq}) \sin \epsilon_l(\omega_{lmpq}) = \frac{3}{2(l-1)} \frac{-A_l J \text{Im} [\bar{J}(\chi)]}{(\text{Re} [\bar{J}(\chi)] + A_l J)^2 + (\text{Im} [\bar{J}(\chi)])^2} \text{Sgn}(\omega_{lmpq}) , \quad (\text{B2})$$

where χ is a shortened notation for the frequency χ_{lmpq} . The coefficients A_l are given by

$$A_l \equiv \frac{(2l^2 + 4l + 3)\mu}{lg\rho R} = \frac{3(2l^2 + 4l + 3)\mu}{4l\pi G\rho^2 R^2} , \quad (\text{B3})$$

where R , ρ , μ , and g are the radius, mean density, unrelaxed rigidity, and surface gravity of the planet, while G is the Newton gravity constant.

¹⁴ We say “a”, because the functional forms of these dependencies depend upon l .

¹⁵ In a hypothetical situation of a planet despinning through a resonance at a constant rate, the appropriate Fourier mode is linear in time. Then the tidal torque, expressed as a function of time, will acquire a similar kink shape. This situation is described in Ferraz-Mello (2013, Figure 7b). Any physically acceptable rheological model must lead to this or similar kind of tidal torque behaviour near a resonance.

The functions

$$\mathcal{R}e[\bar{J}(\chi)] = J + J(\chi\tau_A)^{-\alpha} \cos\left(\frac{\alpha\pi}{2}\right) \Gamma(\alpha + 1) \quad (\text{B4})$$

and

$$\mathcal{I}m[\bar{J}(\chi)] = -J(\chi\tau_M)^{-1} - J(\chi\tau_A)^{-\alpha} \sin\left(\frac{\alpha\pi}{2}\right) \Gamma(\alpha + 1) \quad , \quad (\text{B5})$$

are the real and imaginary parts of the complex compliance $\bar{J}(\chi)$ of the planet. They contain several rheological parameters. Specifically, the notation J stands for the unrelaxed compliance of the mantle, which is inverse to the unrelaxed rigidity μ . The Andrade parameter α is known to be about 0.3 for solid silicates and about 0.14 – 0.2 for partial melts. (We used $\alpha = 0.2$.)

As ever, the notation τ_M stands for the Maxwell time which is the ratio of the mantle’s viscosity η and rigidity μ . For silicate mantles, the values of τ_M may vary greatly, given the exponential dependence of the viscosity upon the temperature. For the Earth, $\tau_M \approx 500$ years.

The so-called Andrade time τ_A was introduced in Efroimsky (2012a,b) as a substitute to the previously used Andrade parameter β . The necessity for that substitution stemmed from the commonly employed β having fractional dimensions and thus lacking a clear physical interpretation. Referring the reader to *Ibid.* for details, we would only recall here that beneath some threshold frequency the friction in the mantle becomes predominantly viscous, while the inelastic processes cease to play a major role. Therefore, at frequencies below that threshold, the mantle’s response becomes close to that of a Maxwell body. Mathematically, this means that below the threshold the parameter τ_A increases rapidly as the frequency goes down. As a result of this, only the first term in (B7) and the first term in (B8) remain relevant, and the resulting complex compliance coincides with that of a Maxwell material.

At the frequencies higher than the threshold, the Andrade time τ_A is comparable to or lower than the Maxwell time τ_M . As can be seen from the expressions (B7) and (B8), in that frequency band the mantle behaves as an Andrade body. The physical reason for this is that at higher frequencies defect-unpinning becomes a dominating mechanism of energy damping.

In our computations, we treated τ_A in the same way as in Makarov et al. (2012) and Makarov (2012): we set $\tau_A = \tau_M$ at the frequencies above the threshold (chosen to be 1 yr^{-1} , like for the solid Earth). Below the threshold, we set τ_A to increase exponentially with the decrease of the frequency, so at low frequencies the rheological model approached the Maxwell one. Numerical runs have shown that the resulting capture probabilities are not

very sensitive to how quickly the switch from the Andrade to Maxwell model is performed (Makarov 2012).

Programming the quality functions, it is practical to divide both the numerator and denominator of (B2) by J^2 :

$$k_l(\omega_{lmpq}) \sin \epsilon_l(\omega_{lmpq}) = \frac{3}{2(l-1)} \frac{-A_l \mathcal{I}}{(\mathcal{R} + A_l)^2 + \mathcal{I}^2} \text{Sgn}(\omega_{lmpq}) \quad , \quad (\text{B6})$$

\mathcal{R} and \mathcal{I} being the *dimensionless* real and imaginary parts of the complex compliance:

$$\mathcal{R} = 1 + (\chi\tau_A)^{-\alpha} \cos\left(\frac{\alpha\pi}{2}\right) \Gamma(\alpha + 1) \quad , \quad (\text{B7})$$

$$\mathcal{I} = -(\chi\tau_M)^{-1} - (\chi\tau_A)^{-\alpha} \sin\left(\frac{\alpha\pi}{2}\right) \Gamma(\alpha + 1) \quad . \quad (\text{B8})$$

These dependencies were used by Makarov et al. (2012), to study the spin-orbit dynamics of the super-Earth GJ581d, and in Makarov (2012), to explore the dynamics of a Mercury-like planet.

C. On the notation “ Q ” used in the CTL tidal model (20 - 25)

An accurate derivation (Williams & Efroimsky 2012) furnishes the following expression for the overall factor entering the CTL expression (20) for the tidal torque:

$$\mathcal{Z} = \frac{3 G M_{star}^2 k_2 \Delta t R^6}{R a^6} = \frac{3 n^2 M_{star}^2 k_2 \Delta t R^5}{(M_{planet} + M_{star}) a^3} \quad . \quad (\text{C1a})$$

Here Δt is the time lag which is, within the CTL model, set to be frequency-independent. In the above expression, it is possible to separate a factor $n \Delta t$:

$$\mathcal{Z} = \frac{3 n M_{star}^2 k_2}{(M_{planet} + M_{star}) a^3} \frac{R^5}{a^3} n \Delta t \approx 3 n M_{star} k_2 \frac{R^5}{a^3} n \Delta t \quad . \quad (\text{C1b})$$

It is this factor of $n \Delta t$ which Correia & Laskar (2004) denoted with $1/Q$ and which we prefer to call $1/“Q”(n)$:

$$n \Delta t = \frac{1}{“Q”(n)} \quad . \quad (\text{C2})$$

Expressed through the so-defined $1/“Q”(n)$, the quantity \mathcal{Z} looks as

$$\mathcal{Z} = \frac{3 n M_{star}^2 k_2}{(M_{planet} + M_{star}) a^3} \frac{R^5}{a^3} \frac{1}{“Q”(n)} \approx \frac{3 n M_{star} k_2}{“Q”(n)} \frac{R^5}{a^3} \quad . \quad (\text{C3})$$

Within the CTL model, it is convenient to introduce the “instantaneous tidal frequency”

$$\chi = 2|\dot{\nu} - \dot{\theta}| , \quad (\text{C4})$$

where ν is the true anomaly. It is also possible to introduce the “instantaneous quality factor” denoted by “ Q ”(χ) and defined through

$$\chi \Delta t = \frac{1}{\text{“}Q\text{”}(\chi)} . \quad (\text{C5})$$

In this case, the expression (C1b) for \mathcal{Z} will be written as

$$\mathcal{Z} = \frac{3 n M_{star}^2 k_2}{M_{planet} + M_{star}} \frac{R^5}{a^3} \frac{n}{\chi} \chi \Delta t \quad (\text{C6a})$$

$$= \frac{3 n M_{star}^2 k_2}{M_{planet} + M_{star}} \frac{R^5}{a^3} \frac{n}{\chi} \frac{1}{\text{“}Q\text{”}(\chi)} \approx \frac{3 n M_{star} k_2}{\text{“}Q\text{”}(\chi)} \frac{R^5}{a^3} \frac{n}{\chi} . \quad (\text{C6b})$$

In the 3:2 resonance (and nowhere else), we have $\chi \approx n$ and therefore “ Q ”(χ) \approx “ Q ”(n). It should be, however, reiterated that the function “ Q ”(χ) = $1/(\chi \Delta t)$ is *not* a quality factor in the ordinary sense of word (Williams & Efroimsky 2012, Section 4). Nor can its particular value “ Q ”(n) be interpreted as such.

REFERENCES

- Archinal, B. A.; A’Hearn, M. F.; Bowell, E.; Conrad, A.; Consolmagno, G. J.; Courtin, R.; Fukushima, T.; Hestroffer, D.; Hilton, J. L.; Krasinsky, G. A.; Neumann, G.; Oberst, J.; Seidelmann, P. K.; Stooke, P.; Tholen, D. J.; Thomas, P. C.; and Williams, I. P. 2011. “Report of the IAU Working Group on Cartographic Coordinates and Rotational Elements: 2009.” *Celestial Mechanics and Dynamical Astronomy*, Vol. **109**, pp. 101 - 135.
- Batygin, K., & Laughlin, G. 2008. “On the dynamical stability of the Solar System.” *ApJ*, Vol. **683**, pp. 1207 - 1216
- Boué, G.; Laskar, J.; & Farago, F. 2012. “A simple model of the chaotic eccentricity of Mercury.” *A&A*, Vol. **548**, p. A43
- Bretagnon, P. 1974. “Termes à longues périodes dans le système solaire.” *A&A*, Vol. **30**, pp. 141 - 154

- Bretagnon, P. 1982. “Theory for the motion of all the planets - The VSOP82 solution.” *A&A*, Vol. **114**, pp. 278 - 288
- Castillo-Rogez, J.C.; Efroimsky, M.; & Lainey, V. 2011. “The tidal history of Iapetus: Spin dynamics in the light of a refined dissipation model.” *J. Geophys. Res.*, Vol. **116**, E09008
- Colombo, G. 1965. “Rotational period of the planet Mercury.” *Nature*, Vol. **208**, p. 575
- Correia, A.C.M., & Laskar, J. 2004. “Mercury’s capture into the 3/2 spin-orbit resonance as a result of its chaotic dynamics.” *Nature*, Vol. **429**, pp. 848 - 850
- Correia, A.C.M., & Laskar, J. 2009. “Mercury’s capture into the 3/2 spin-orbit resonance including the effect of core-mantle friction.” *Icarus*, Vol. **201**, pp. 1 - 11
- Correia, A.C.M., & Laskar, J. 2010. “Long-term evolution of the spin of Mercury I. Effect of the obliquity and core-mantle friction.” *Icarus*, Vol. **205**, pp. 338 - 355
- Correia, A.C.M., & Laskar, J. 2012. “Impact cratering on Mercury: Consequences for the spin evolution.” *ApJ*, 751:L43
- Dahlquist G. & Björck Å. 2008. *Numerical Methods in Scientific Computing*, Vol. 1. SIAM, Philadelphia, pp. 351-520 (Chapter 4)
- Danby, J.M.A. 1962. *Fundamentals of Celestial Mechanics*. MacMillan, New York
- Darwin, G. H. 1879. “On the precession of a viscous spheroid and on the remote history of the Earth.” *Philosophical Transactions of the Royal Society of London*, Vol. **170**, pp. 447 - 530
- Dobrovolskis, A.R. 2007. “Spin states and climates of eccentric exoplanets.” *Icarus*, Vol. **192**, pp. 1 - 2
- Duriez L. 2002. Cours de mécanique céleste classique, http://lal.univ-lille1.fr/mecanique_celeste.html
- Efroimsky, M., & Lainey, V. 2007. “Physics of bodily tides in terrestrial planets and the appropriate scales of dynamical evolution.” *J. Geophys. Res.*, 112, E12003
- Efroimsky, M., & Williams, J.G. 2009. “Tidal torques: a critical review of some techniques.” *Celestial Mechanics and Dynamical Astronomy*, Vol. **104**, pp. 257 - 289

- Efroimsky, M. 2012a. “Bodily tides near spin-orbit resonances.” *Celestial Mechanics and Dynamical Astronomy*, Vol. **112**, pp. 283 - 330
Extended version: <http://arxiv.org/abs/1105.6086>
- Efroimsky, M. 2012b. “Tidal dissipation compared to seismic dissipation: in small bodies, earths, and superearths.” *The Astrophysical Journal*, Vol. **746**, id. 150
doi:10.1088/0004-637X/746/2/150 <http://arxiv.org/abs/1105.3936>
ERRATA: *ApJ*, Vol. **763**, id. 150 (2013)
- Efroimsky, M., & Makarov, V.V. 2013. “Tidal friction and tidal lagging. Applicability limitations of a popular formula for the tidal torque.” *ApJ*, 764:26
- Eggleton, P. P.; Kiseleva, L. G.; and Hut, P. 1998. “The equilibrium tide model for tidal friction.” *The Astrophysical Journal*, Vol. **499**, pp. 853 - 870
- Ferraz-Mello, S.; Rodríguez, A.; & Hussmann, H. 2008. “Tidal friction in close-in satellites and exoplanets: The Darwin theory re-visited.” *Celestial Mechanics and Dynamical Astronomy*, Vol. **101**, pp. 171 - 201
- Ferraz-Mello, S. 2013. “Tidal synchronization of close-in satellites and exoplanets. A rheophysical approach.” *Celestial Mechanics and Dynamical Astronomy*, Vol. **116**, pp. 109 - 140
- Galassi, M.; Davies, J.; Theiler, J.; Gough, B.; Jungman, G.; Alken, P.; Booth, M.; & Rossi, F. 2009. *GNU Scientific Library Reference Manual* (v1.12), 3rd ed. Network Theory Ltd., Bristol
- Goldreich, P., & Peale, S. 1966. “Spin-orbit coupling in the Solar System.” *AJ*, Vol. **71**, pp. 425 - 438
- Goldreich, P., and Peale, S.J. 1968. “The Dynamics of Planetary Rotations.” *Annual Review of Astronomy and Astrophysics*, Vol. **6**, pp. 287 - 320
- Hairer E., Nørsett S.P. & Wanner G., 1987, Solving Ordinary Differential Equations. I: Nonstiff Problems, Springer Series in computational Mathematics, Springer-Verlag, Berlin
- Henrard J., 1982, Capture into resonance: an extension of the use of adiabatic invariants, *Celestial Mechanics*, 27, 3-22
- Hut, P. 1981. “Tidal evolution in close binary systems.” *Astronomy & Astrophysics*, Vol. **99**, pp. 126 - 140

- Karato, S.-i., and Spetzler, H. A. 1990. “Defect Microdynamics in Minerals and Solid-State Mechanisms of Seismic Wave Attenuation and Velocity Dispersion in the Mantle.” *Reviews of Geophysics*, Vol. **28**, pp. 399 - 423
- Kaula, W.M. 1964. “Tidal dissipation by solid friction and the resulting orbital evolution.” *Reviews of Geophysics*, 2, 661 - 685
- Laskar J., 1986, Secular terms of classical planetary theories using the results of general theory, *A&A*, 157, 59-70
- Laskar, J. 1988. “Secular evolution of the solar system over 10 million years.” *A&A*, 198, 341 - 362
- Laskar J., 1989, A numerical experiment on the chaotic behaviour of the solar system, *Nature*, 338, 237
- Laskar, J. 2008. “Chaotic diffusion in the Solar System.” *Icarus*, 196, 1 - 15
- Laskar, J., & Gastineau, M. 2009. “Existence of collisional trajectories of Mercury, Mars and Venus with the Earth.” *Nature*, 459, 817 - 819
- Laskar, J.; Fienga, A.; Gastineau, M.; & Manche, H. 2011. “La2010: a new orbital solution for the long-term motion of the Earth.” *A&A*, Vol. **532**, p. A89
- MacDonald, G.J.F. 1964. “Tidal friction.” *Reviews of Geophysics*, Vol. **2**, pp. 467 - 541
- Makarov, V.V. 2012. “Conditions of passage and entrapment of terrestrial planets in spin-orbit resonances.” *ApJ*, 752:73
- Makarov, V.V.; Berghea, C.; & Efroimsky, M. 2012. “Dynamical evolution and spin-orbit resonances of potentially habitable exoplanets. The case of GJ 581d.” *ApJ*, 761:83
- Makarov, V.V., & Efroimsky, M. 2013. “No pseudosynchronous rotation for terrestrial planets and moons.” *ApJ*, 764:27
- Malhotra R., 1991, Tidal origin of the Laplace Resonance and the resurfacing of Ganymede, *Icarus*, Vol. **94**, pp. 399 - 412
- Margot, J.-L.; Peale, S.J.; Jurgens, R.F.; Slade, M.A.; & Holin, I.V. 2007. “Large longitude libration of Mercury reveals a molten core.” *Science*. Vol. **316**, pp. 710 - 714
- Margot, J.-L.; Peale, S.J.; Solomon, S.C.; Hauck II, S.A.; Ghigo, F.D.; Jurgens, R.F.; Yseboodt, M.; Giorgini, J.D.; Padovan, S.; & Campbell, D.B. 2012. “Mercury’s moment of inertia from spin and gravity data.” *J. Geophys. Res.*, Vol. **117**, E00L09

- Mignard, F. 1979. “The Evolution of the Lunar Orbit Revisited. I.” *The Moon and the Planets*. Vol. **20**, pp. 301 - 315
- Mignard, F. 1980. “The Evolution of the Lunar Orbit Revisited. II.” *The Moon and the Planets*. Vol. **23**, pp. 185 - 201.
- Murray, C.D., & Dermott, S.F. 2000, *Solar System Dynamics*, Cambridge University Press
- Nobili A.M., Milani A., Carpino M. 1989. “Fundamental frequencies and small divisors in the orbits of the outer planets.” *A&A*, Vol. **210**, pp. 313 - 336
- Noyelles, B., & Lhotka, C. 2013. “The influence of orbital dynamics, shape and tides on the obliquity of Mercury.” Submitted
<http://arxiv.org/abs/1211.7027>
- Peale, S.J., & Boss, A.P. 1977. “A spin-orbit constraint on the viscosity of a Mercurian liquid core.” *J. Geophys. Res.*, Vol. **82**, pp. 743 - 749
- Pettengill, G.H., & Dyce, R.B. 1965. “A radar determination of the rotation of the planet Mercury.” *Nature*, Vol. **206**, p. 1240
- Press, W.H.; Teutolski, S.A.; Vetterling, W.T.; & Flannery, B.P. 1992. *Numerical Recipes*. Cambridge University Press
- Quinn, T.R.; Tremaine, S.; & Duncan, M. 1991. “A three million year integration of the earth’s orbit.” *AJ*, Vol. **101**, pp. 2287 - 2305
- Rasio, F.A.; Tout, C. A.; Lubow, S. H.; and Livio, M. 1996. “Tidal Decay of Close Planetary Orbits.” *The Astrophysical Journal*, Vol. **470**, pp. 1187 - 1191
- Singer, S. F. 1968. “The Origin of the Moon and Geophysical Consequences.” *The Geophysical Journal of the Royal Astronomical Society*, Vol. **15**, pp. 205 - 226.
- Sonneveld, P. 1969. “Errors in cubic spline interpolation.” *Journal of Engineering Mathematics*, Vol. **3**, pp. 107-117
- Sussman, G.J., & Wisdom, J. 1992. “Chaotic evolution of the solar system.” *Science*, Vol. **257**, pp. 56 - 62
- Wieczorek, M.A.; Correia, A.C.M.; Le Feuvre, M.; Laskar, J.; & Rambaux, N. 2012. “Mercury’s spin-orbit resonance explained by initial retrograde and subsequent synchronous rotation.” *Nature Geoscience*, Vol. **5**, pp. 18 - 21

Williams, J.G., & Efroimsky, M. 2012. “Bodily tides near the 1:1 spin-orbit resonance: correction to Goldreich’s dynamical model.” *Celestial Mechanics and Dynamical Astronomy*, Vol. **114**, pp. 387 - 414